Aalborg Universitet

AALBORG UNIVERSITY
DENMARK

Forecasting Spatiotemporal Dynamics of Daytime Surface Urban Cool Islands in Response to Urbanization in Drylands

Case Study of Kerman and Zahedan Cities, Iran

Firozjaei, Mohammad Karimi; Mijani, Naeim; Fathololoumi, Solmaz; Arsanjani, Jamal Jokar

Published in:
Remote Sensing

DOI (link to publication from Publisher):
10.3390/rs16234416

Creative Commons License
CC BY 4.0

Publication date:
2024

Document Version
Publisher's PDF, also known as Version of record

Link to publication from Aalborg University

Citation for published version (APA):
Firozjaei, M. K., Mijani, N., Fathololoumi, S., & Arsanjani, J. J. (2024). Forecasting Spatiotemporal Dynamics of Daytime Surface Urban Cool Islands in Response to Urbanization in Drylands: Case Study of Kerman and Zahedan Cities, Iran. *Remote Sensing*, *16*(23), Article 4416. https://doi.org/10.3390/rs16234416

General rights
Copyright and moral rights for the publications made accessible in the public portal are retained by the authors and/or other copyright owners and it is a condition of accessing publications that users recognise and abide by the legal requirements associated with these rights.

- Users may download and print one copy of any publication from the public portal for the purpose of private study or research.
- You may not further distribute the material or use it for any profit-making activity or commercial gain
- You may freely distribute the URL identifying the publication in the public portal -

Take down policy
If you believe that this document breaches copyright please contact us at vbn@aub.aau.dk providing details, and we will remove access to the work immediately and investigate your claim.

Downloaded from vbn.aau.dk on: February 07, 2025

remote sensing

MDPI

Article

Forecasting Spatiotemporal Dynamics of Daytime Surface Urban Cool Islands in Response to Urbanization in Drylands: Case Study of Kerman and Zahedan Cities, Iran

Mohammad Karimi Firozjaei [1], Naeim Mijani [2], Solmaz Fathololoumi [3] and Jamal Jokar Arsanjani [4,*]

[1] Tourism Faculty, University of Tehran, Tehran 1417964743, Iran; mohammad.karimi.f@ut.ac.ir
[2] Department of Geography and Environment, Western University, London, ON N6A 5C2, Canada; nmijani@uwo.ca
[3] School of Environmental Sciences, University of Guelph, Guelph, ON N1G 2W1, Canada; sfatholo@uoguelph.ca
[4] Geoinformatics Research Group, Department of Planning and Development, Aalborg University Copenhagen, A.C. Meyers Vænge 15, DK-2450 Copenhagen, Denmark
* Correspondence: jja@plan.aau.dk

Abstract: Urban micro-climate plays an important role in human activities and in ensuring public health. For instance, the urban heat island effect is crucial to the thermal comfort of citizens and tourists, similar to the urban cool island effect's importance on human and infrastructure resilience. Approximately 35% of global big cities are located in drylands. While existing research has focused on the spatial and temporal changes of surface urban cooling island intensity (SUCII) in drylands in the past, there is a gap in predicting the future spatiotemporal changes in SUCII for cities within these dryland regions. This study aims to forecast the spatiotemporal dynamics of daytime SUCII of representative growing cities with a dry and cold climate. Kerman and Zahedan cities, which are undergoing large urbanization and have harsh hot summer climates, were selected as the study area. Landsat 5 and 8 images and products were utilized for six timestamps within the timeframe of 1986–2023. Various methods, including a random forest algorithm, spectral indices, Cellular Automata-Markov (CA-Markov) model, the cross-tabulation model, and spatial overlay and zonal statistics, were employed to assess and model the spatiotemporal changes in SUCII. Initially, historical land cover maps, land surface temperature (LST), surface biophysical characteristics, and SUCII data were prepared, and their spatiotemporal changes were evaluated. Then, projected maps for these variables for the year 2045 were produced. The results indicated that the built-up areas, bare lands, and green spaces of Kerman (Zahedan) city in 1986 were 26.6 km^2 (17.6 km^2), 103 km^2 (92.5 km^2), and 44.4 km^2 (5.6 km^2), respectively, and these values reached 99.3 km^2 (41.9 km^2), 61.2 km^2 (70.7 km^2), and 13.5 km^2 (3.2 km^2) in 2023. The built-up lands area of Kerman (Zahedan) city is expected to increase by approximately 26% (36%) by 2045, while bare land and green space are expected to decrease by about 32% (20%) and 39% (31%), respectively. The greatest rise in average LST of Kerman (Zahedan) city is associated with the conversion of green spaces to barren land, resulting in a notable increase of 5.5 °C (4.3 °C) in 1986–2023. The conversion of barren land to built-up land in Kerman (Zahedan) city has led to a decrease of 4.6 °C (3.8 °C) in LST. The SUCII of Kerman (Zahedan) city for 1986, 1994, 2001, 2008, 2015, and 2023 were −0.3 °C (0.9 °C), −0.8 °C (0.4 °C), −1.4 °C (−0.5 °C), −1.9 °C (−1.5 °C), −2.6 °C (−2.5 °C), and −3.2 °C (−3.4 °C), respectively. The projected SUCII in Kerman (Zahedan) city for 2045 is about −4.3 °C (−4.5 °C), indicating an increasing trend in SUCII in the future. The area of zones without SUCII in Kerman (Zahedan) city decreased by 44.8 Km^2 (54.8 Km^2) from 1986 to 2023, while the areas of low, medium, and high SUCII classes increased by 9.1 Km^2 (9.9 Km^2), 10.9 Km^2 (11.9 Km^2), and 24.8 Km^2 (33.1 Km^2), respectively. The area of non-SUCII and high SUCII classes of Kerman (Zahedan) city in 2045 is expected to decrease by 31.5 Km^2 (12.0 Km^2) and increase by 51.2 Km^2 (9.5 Km^2) compared with 2023. The findings of this research indicate that the physical growth of cities in drylands can lead to the moderation of LST, contrary to mechanisms in humid and wet regions.

check for updates

Citation: Firozjaei, M.K.; Mijani, N.; Fathololoumi, S.; Arsanjani, J.J. Forecasting Spatiotemporal Dynamics of Daytime Surface Urban Cool Islands in Response to Urbanization in Drylands: Case Study of Kerman and Zahedan Cities, Iran. *Remote Sens.* **2024**, *16*, 4416. https://doi.org/10.3390/rs16234416

Academic Editor: Ashraf Dewan

Received: 28 August 2024
Revised: 25 September 2024
Accepted: 20 November 2024
Published: 26 November 2024

Copyright: © 2024 by the authors. Licensee MDPI, Basel, Switzerland. This article is an open access article distributed under the terms and conditions of the Creative Commons Attribution (CC BY) license (https://creativecommons.org/licenses/by/4.0/).

Keywords: land surface temperature; urban climate; urban growth; land cover changes; surface biophysical characteristics; remote sensing

1. Introduction

As cities grow physically due to population growth, economic, social, resilience, and sustainability factors continue to grow and cause cascading and compound effects on natural resources, the environment, surface energy balance, water ecosystems, atmospheric conditions, ecosystems, and climate [1–3]. The cumulative negative impacts of unsustainable urban development practices ultimately will lead to a decline in the quality of human life in urban and non-urban environments, particularly in developing countries with classical urban planning agendas [4–8]. To manage the adverse effects of population growth and urban expansion, the implementation of smart and sustainable urban strategies is essential [7,9–11]. In this regard, international communities in light of the UN Sustainable Development Goals (UN-SDGs) are seeking innovative and sustainable solutions for urban development and optimal resource management to maintain a balance between urban development and environmental conservation for a sustainable future.

Changes in land cover are among the primary effects of the physical growth of cities on the environment and natural resources, and they hold significant importance [12–15]. These changes typically occur due to construction activities, urban development, and land use alterations. The impacts can induce various alterations in the biophysical characteristics of the land surface, including surface permeability, vegetation cover, and imperviousness, leading to irreversible unpleasant consequences [16–18]. The outcomes of these changes exacerbate anomalies in urban environment thermal quality [19–22] and also influence vegetation phenology [23,24] and vegetation growth [25]. Therefore, monitoring and predicting land cover changes resulting from urban growth and their impact on urban environment thermal quality not only enhances our comprehension of the effects stemming from such changes but also facilitates the implementation of primitive measures to mitigate these effects [26–31]. This, in turn, assists climate planners, stakeholders, and relevant decision makers in developing more effective management strategies to control environmental thermal stress and alleviate its adverse consequences. Additionally, studies on this subject contribute to various UN- SDGs, underscoring its potential to drive global sustainability initiatives. In summary, the results of this study contribute to the sustainable well-being of urban environment thermal quality and the quality of life for its inhabitants.

The difference in energy balance between urban and peri-urban areas arises from variations in surface characteristics [1,32,33]. Disparities in surface features between urban and non-urban areas include factors such as heat absorption capacity, surface albedo, permeability, vegetation cover density, and three-dimensional geometry of structures, contributing to temperature differences between urban and non-urban areas [34–37]. The magnitude of this temperature difference varies in regions with different climatic conditions [16,38–40]. In humid and temperate climates, increased building density, widespread use of heat-absorbing materials like asphalt and concrete, reduced surface albedo, and overall vegetation constraints intensify heat retention [16,31,37,41]. These factors ultimately lead to higher LST in urban areas compared with non-urban areas, creating the surface urban heat island (SUHI) effect [42–45]. The SUHI effect has been extensively evaluated in past research, emphasizing the importance of urban planning and environmental management in mitigating the adverse effects of SUHIs.

The impact of urban growth and the conversion of natural lands into built-up areas in semi-arid and arid regions differs. Placing dry bare lands around cities in semi-arid and arid regions results in lower daytime LST in urban areas compared with non-urban areas [46–50]. The cooler daytime LST in urban areas may be attributed to factors such as soil moisture levels in the urban area, cooling effects from plant transpiration, shading from the crowns of trees and buildings, and the presence of open water bodies like urban

lakes and rivers. This contrasts with the barren lands surrounding the city, which have dry surfaces with minimal vegetation cover and shade. This cooling effect is termed the surface urban cooling island (SUCI) [51–53]. Some past studies have focused on assessing the SUCI effect and its spatiotemporal changes. Their results indicate that the physical growth of cities in dry and semi-arid regions can lead to the moderation of LST, contrary to mechanisms in humid and temperate areas [46–53].

The phenomenon of SUCI is not limited to arid regions but also occurs in other climate zones such as temperate, tropical, and humid areas, though the patterns, intensity, and mechanisms of formation vary across these regions. In humid and temperate climates, the SUCI effect often emerges due to the cooling effects of water bodies and extensive vegetation, whereas in arid zones, they largely depend on strategic urban planning, green infrastructure, and reflective surfaces. A comparative analysis of SUCIs across different climate zones would contribute to a broader understanding of this phenomenon and offer more effective strategies for managing urban heat on a global scale, particularly in response to climate change. As for the relationship between urbanization and the formation of SUCIs, urban expansion can have both positive and negative impacts. On the one hand, the expansion of cities into suburban areas and the development of green spaces and open areas can foster the formation of SUCIs. On the other hand, the densification of urban areas and the reduction of green cover in central city zones can inhibit their development. Implementing innovative urban design techniques—such as green roofs, reflective materials, urban parks, and low-heat-absorbing building materials—can help reinforce SUCI formation. These strategies are especially critical in arid regions, where high daytime temperatures and limited water resources present significant challenges. By improving urban thermal conditions, these measures can mitigate the effects of urban heat islands and enhance the overall livability of cities.

A detailed and comprehensive examination of environmental conditions in urban areas requires integrated, accurate, and extensive data and information. Satellite data, due to its ability to provide information over a long period, stay up-to-date, and capture data at various local, regional, and global scales, plays a crucial role in assessing spatial and temporal changes in the physical growth of cities, their surface characteristics, and their thermal effects [15,16,36,38,41,54]. Understanding and mitigating SUHI and SUCI effects necessitates accurate and comprehensive measurements of LST. Recent decades have witnessed significant advancements in remotely sensed thermal infrared (TIR) data and modeling techniques, enabling the derivation of LST with varying spatial and temporal resolutions [55–58]. To gain deeper insights into the spatial and temporal dynamics of urban heat, researchers have increasingly leveraged TIR remote sensing to estimate LST across extensive urban areas [59–62]. While earlier studies primarily relied on coarse-resolution data from sensors like Advanced Very High Resolution Radiometer (AVHRR) and Moderate Resolution Imaging Spectroradiometer (MODIS), the availability of higher-resolution imagery from platforms such as Advanced Spaceborne Thermal Emission and Reflection Radiometer (ASTER), Landsat, and ECOsystem Spaceborne Thermal Radiometer Experiment on Space Station (ECOSTRESS) has facilitated more detailed analyses of urban thermal environments [41,59,63–69]. Analyzing historical satellite data helps us understand patterns of urban growth and temperature changes in cities, evaluating their impacts on the environment and the quality of life for residents. Predicting future changes based on these assessments is also important. Considering the projected urban growth and analyzing spatial and temporal changes allows for the development of optimal strategies to enhance urban heat management.

Our literature review found several studies on SUHI and SUCI that include (a) quantitative assessments of SUHI and SUCI methods [1,37,42,60,70–72], (b) spatial and temporal changes in SUHIs and SUCIs [36,41,73–78], (c) parameters influencing the formation and intensity of SUHIs and SUCIs [38,79–84], (d) methods to mitigate the negative effects of SUHIs [85–87], and (e) the prediction of spatial and temporal changes in SUHIs [21,30,31,88–90]. For instance, Firozjaei et al. [31] predicted the spatial and temporal

changes in SUHIs for Babol city in the year 2045. The study's results indicated that 67% of the built-up lands in Babol experienced SUHI effects in 2018, which will increase to 72% in 2045. Wang et al. [21] predicted the spatial and temporal changes in SUHIs for Nanjing city in the years 2030 and 2050 using the CA-Markov model. Their results showed that areas with high SUHI intensity in 2030 and 2050 will mainly be distributed in the central region of Nanjing, resulting from the distribution of built-up lands. Liu et al. [91] predicted the intensity of SUHIs in Shuchang, China, for the year 2023 based on a future land use simulation model and regression analysis. The study revealed a significant correlation between the land use index of urban areas and SUHI. A regression analysis showed that the effects of SUHIs in this city will decrease in 2030. Kiavarz et al. [29] predicted the SUHI intensity in Tehran for the years 2026, 2032, and 2045. Their results showed that SUHI intensity in Tehran was minimal in 1985 but increased to nearly one-third of the built-up lands in the city in 2019. The predicted results indicate that approximately 38%, 45%, and 51% of the built-up lands in Tehran will be under the influence of SUHIs in 2026, 2032, and 2045, respectively.

In summary, previous studies have predominantly focused on SUHIs rather than SUCIs. Additionally, a notable finding is that 35% (586 of 1692) of global big cities are located in drylands (dry sub-humid, semi-arid, arid, and hyper-arid) (https://wad.jrc.ec.europa.eu/arididyurban (accessed on 15 February 2024)). Most research has concentrated on the spatial and temporal changes of SUCIs in drylands in the past, and there is a gap in predicting the future spatiotemporal changes in SUCIs for cities in dryland areas. The lack of attention to forecasting SUCI dynamics in these regions presents an opportunity for future research. This study aims to address this gap by forecasting the spatiotemporal dynamics of daytime SUCI intensity (SUCII) in response to the urbanization process in drylands. The results of such forecasts can serve as valuable tools for urban planners in optimizing future urban development plans.

2. Study Area

The first study area encompasses Kerman city and its surrounding regions, with a total area of 174 km^2, located at 57.06°N and 30.2°E, and the city serves as the capital of the Kerman province of Iran (Figure 1). It serves as a significant hub for industrial, political, cultural, scientific, and technological activities in the southeast of Iran. The city's average elevation above sea level is 1756 m, and it is categorized as dry and semi-arid according to the Dumatron climate classification. With an annual average precipitation of 135 mm, Kerman often experiences extremely hot summers and intense sandstorms in the spring, given its proximity to the Lut Desert. The highest average monthly temperature in Kerman city is 32.9 °C in July. The difference between the highest and lowest average monthly temperatures in this city is 24.5 °C, with January recording the lowest average monthly temperature. The urban population of Kerman is approximately 718,000, making it the tenth most populous city in Iran. Over the past four decades, migration from southern counties of the Kerman province and neighboring provinces to Kerman city has contributed to the city's physical growth and land cover changes in the surrounding areas.

The second study area comprises the city of Zahedan and its surrounding regions, covering an area of 100.5 square kilometers. Geographically, it is located at 60.85 degrees east longitude and 29.49 degrees north latitude. This city is one of Iran's metropolises and is the capital of Sistan and Baluchestan Province. Zahedan is situated in Zahedan County and is bordered by Hamoun County to the north, Taftan County to the south, Afghanistan and Pakistan to the east, and Fahraj County to the west. Zahedan is a newly established city located 517 km east of Kerman. Due to a significant population increase in recent years, the city has experienced rapid and substantial urban land expansion. Based on the 2016 Iranian census, Zahedan's population was 587,730, making it the 12th most populous city in Iran. The climate of Zahedan is hot and arid, although nights in the summer tend to be cooler. For most of the year, the weather is hot and dry, with very hot days and relatively cool nights in the summer. Snowfall is rare in the city, with the highest precipitation occurring

in winter. In December and January, the weather is generally cool with cold nights. The highest average monthly temperature in Zahedan city is 35.3 °C in July. The difference between the highest and lowest average monthly temperatures in this city is 25.9 °C, with January having the lowest average monthly temperature. Zahedan is situated in a large basin surrounded by various mountains. Among the most important mountains in the city are Ashtran (3012 m), Anjirdan (2255 m), Jiko, Pirkhan (2221 m), and Maleksiah.

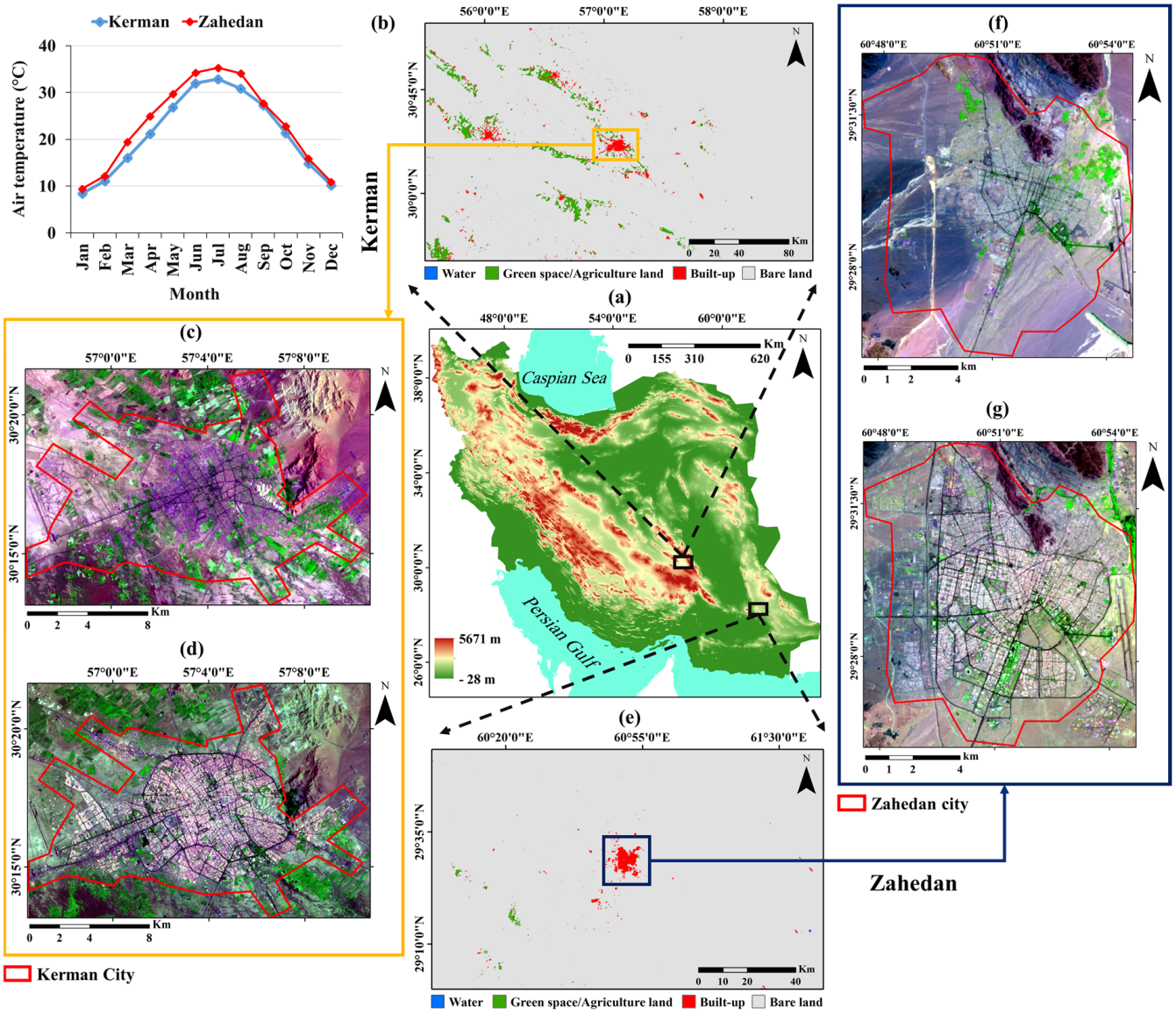

Figure 1. Maps: (**a**) Geographical location of the study area on the digital elevation model (DEM) map; (**b**) geographical location of Kerman city on the land cover map; (**c**) Landsat 5 color composite image (SWIR 2, NIR, Blue) of Kerman city from 1986; (**d**) Landsat 8 color composite image (SWIR 2, NIR, Blue) of Kerman city from 2023; (**e**) Geographical location of Zahedan city on the land cover map; (**f**) Landsat 5 color composite image (SWIR 2, NIR, Blue) of Zahedan city from 1986; (**g**) Landsat 8 color composite image (SWIR 2, NIR, Blue) of Zahedan city from 2023.

3. Data and Methods

3.1. Data

In this study, multi-temporal Landsat 5 and 8 satellite images were utilized for the years 1986, 1994, 2001, 2008, 2015, and 2023. Launched in 1984 in collaboration with NASA and the United States Geological Survey (USGS), Landsat 5 observed the Earth's surface for 28 years. The satellite image from Landsat 5 comprises six bands in the reflective wavelength range, one thermal band, and one panchromatic band, with an 8-bit radiometric resolution. Landsat 8, launched in 2013 as part of the Landsat satellite series, features two operational Earth imagers (OLIs) and a thermal infrared sensor (TIRS). The OLI sensor consists of 8 reflective bands and 1 panchromatic band, while the TIRS sensor has 2 thermal bands situated in the atmospheric window between the wavelengths of 10 and 12 μm, with a 16-bit radiometric resolution. The spatial and temporal resolution of Landsat 5 and 8 satellite images is 30 m and 16 days, respectively, with a referencing error of less than 12 m. Due to their sensors being capable of recording information in both the reflective and thermal ranges of electromagnetic waves, long-term temporal coverage, and appropriate spatial resolution, Landsat satellite images are widely employed in various environmental and urban applications [30,54,92–97].

In this study, Landsat products were employed to generate maps of surface characteristics for different years. Landsat Collection 2 Level 2 surface reflectance and Landsat Collection 2 Level 2 surface temperature products, with a spatial resolution of 30 m, were used. The cloud coverage for all selected images was less than 10%. A median image, derived from cloud-free images available for the study area from the beginning of May to the end of August each year, was used to map various surface characteristics. These images can be accessed on the USGS website (https://earthexplorer.usgs.gov (accessed on 15 February 2024)). In this study, the median image for different years was calculated using the Google Earth Engine (GEE) platform.

To create training and test data for land cover classification and evaluation operations, data were collected based on Landsat color composite images and high-spatial resolution images such as Google Earth. On each date, around 600 pixels were utilized as training data, while an additional 300 pixels were allocated for test data for each of the land cover classes.

3.2. Methods

The general stages of the method are illustrated in Figure 2. To achieve the research objective, seven main stages have been implemented. In the first step, land cover maps for different years were prepared using the random forest classification algorithm. In the second step, maps of surface biophysical characteristics, including greenness, imperviousness, and wetness, for different years were generated using spectral indices such as Normalized Difference Vegetation Index (NDVI), Normalized Difference Built-up Index (NDBI), and Normalized Difference Water Index (NDWI). Additionally, LST maps for Kerman and Zahedan cities were extracted using the Landsat Collection 2 surface temperature product. In the fourth step, spatial and temporal changes in land cover were assessed using the cross-tabulation model, and changes in surface biophysical characteristics and LST were evaluated using the subtraction operator. In the fifth stage, the impact of changes in land cover and surface biophysical characteristics on LST changes in Kerman and Zahedan cities was calculated and compared. In the sixth stage, predictive maps of land cover and LST for the future year were prepared based on the CA-Markov model. In the seventh stage, the spatiotemporal dynamics patterns of SUCII for different years in Kerman and Zahedan cities were quantified and compared within past and future time intervals.

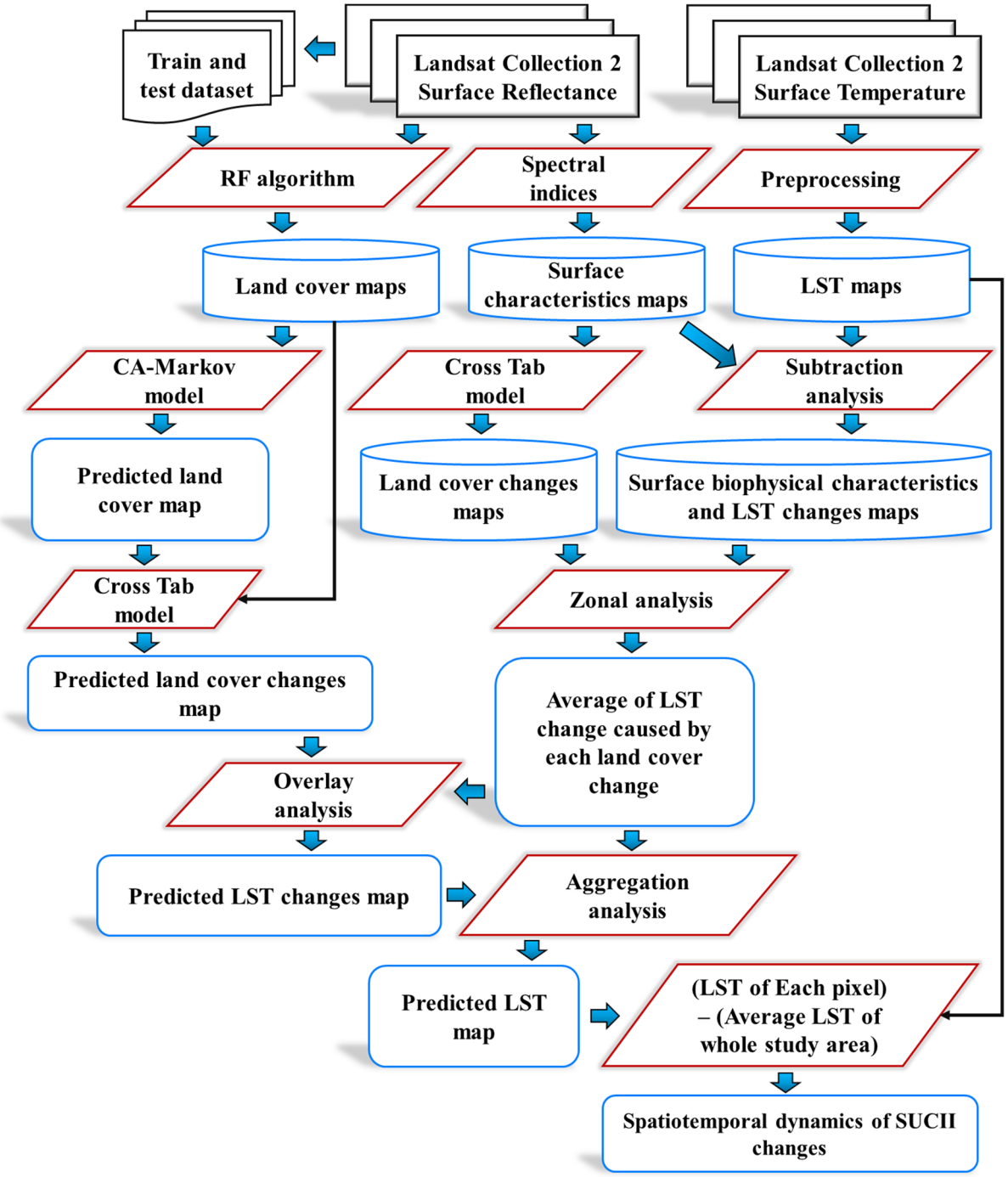

Figure 2. Flowchart of study method.

3.2.1. Land Cover Classification

The types and number of land cover classes in Kerman and Zahedan cities were determined based on the author's information, field visits, and visual interpretation of satellite images. In this study, the random forest algorithm was employed to generate land cover maps for different years [98–100]. The spectral bands of Landsat satellite images, including blue, green, red, near-infrared, SWIR 1, and SWIR 2, were used as effective features in the random forest algorithm for land cover classification. The implementation of the random forest algorithm as a supervised method requires training data. In this stage, a training dataset was created for the algorithm's training and calibration, using visual interpretations of Landsat color composite images and high-spatial resolution satellite images in different years. The testing dataset was also established for evaluating the

accuracy of the produced land cover maps. Overall accuracy was used as a general criterion for assessing the accuracy of the land cover maps. After generating the land cover maps, the area corresponding to each land cover class in different years was calculated, and the trend of changes was evaluated. To determine land cover changes in the study period, land cover maps produced in 1986 and 2023 were compared using the cross-tabulation model. The land cover maps and their accuracy assessment, as well as the land cover change maps, were prepared using ENVI 5.3 software.

- Prediction of future land cover map

In this study, the CA-Markov model was employed for predicting the future land cover patterns. Both Markov chain and CA are discrete dynamic models in space and time [101–103]. In the CA-Markov model, the Markov chain process transforms temporal changes between land cover classes based on transition probabilities, while spatial changes are controlled by locally defined rules through the CA spatial filter. The details of this method for predicting land cover were presented in Arsanjani et al. [104] and Firozjaei et al. [105]. To generate the land suitability map for the transformation to built-up lands, criteria such as distance from built-up lands, distance from road networks, distance from agricultural areas, distance from green spaces, distance from the city center, and slope were utilized. Parks and protected areas within Kerman and Zahedan cities were considered as constraints. The analytic hierarchy process (AHP) model [106,107] was employed to determine the weights of these criteria, and the weighted linear combination (WLC) method was used to combine the criterion values and weights. Initially, by implementing the CA-Markov model on land cover maps for the years 1994 and 2008, the land cover map for 2023 was predicted. The accuracy of the predicted land cover map using this model was calculated by comparing it with the land cover map obtained from satellite imagery in 2023. Subsequently, by inputting the land cover maps for the years 2001 and 2023 into the CA-Markov model, the land cover map for Kerman and Zahedan cities in 2045 was predicted. TerrSet 2020 software was used for implementing the CA-Markov model. Finally, the changes in land cover between 2023 and 2045 were investigated using the cross-tabulation model.

3.2.2. Extraction of Surface Biophysical Characteristics

In this study, surface characteristics, including vegetation, moisture, and imperviousness, were extracted using the NDVI, NDBI, and NDWI, respectively. These indices were calculated using the reflective bands of Landsat satellite images in different years. These maps were produced on the GEE platform.

- NDVI

The NDVI serves as an indicator of surface greenness and vegetation information [108]. It stands out as one of the most crucial metrics in remote sensing and environmental monitoring, employed to evaluate and visualize alterations in vegetation cover within a specified area. This index is derived by amalgamating satellite data from two distinct wavelengths, one in the near-infrared and the other in the red spectrum. NDVI values span from -1 to 1, where positive values near 1 signify regions with robust vegetation and heightened photosynthetic activity. Conversely, negative values near -1 indicate areas with minimal or no vegetation, such as water surfaces, and values approximating 0 denote regions with sparse or bare land cover. In essence, NDVI proves indispensable for tracking changes in land cover, detecting drought conditions, overseeing agricultural productivity, managing natural resources, and facilitating environmental studies. Through the analysis of fluctuations in this index, valuable insights into the condition of plants and the environment can be gleaned. The NDVI is calculated using Equation (1):

$$\mathrm{NDVI} = \frac{\rho_{\mathrm{NIR}} - \rho_{\mathrm{Red}}}{\rho_{\mathrm{NIR}} + \rho_{\mathrm{Red}}} \quad (1)$$

where ρ_{NIR} and ρ_{Red} represent the near-infrared and red bands, respectively.

- NDBI

The NDBI provides information on land cover, specifically the percentage of impervious surfaces, which include bare and built-up lands [109]. NDBI plays a crucial role in analyzing urban changes and development. The index is computed using satellite data from two different bands, one associated with near-infrared and the other with thermal infrared radiation. Positive NDBI values indicate built-up and urbanized areas, while values that are close to zero or that are negative suggest less developed and more permeable regions. This information is valuable for sustainable urban development management, urban change analysis, and urban resource planning. The NDBI was calculated based on Equation (2):

$$\mathrm{NDBI} = \frac{\rho_{\mathrm{SWIR}} - \rho_{\mathrm{NIR}}}{\rho_{\mathrm{SWIR}} + \rho_{\mathrm{NIR}}} \quad (2)$$

where ρ_{SWIR} and ρ_{NIR} represent the short-wave infrared and near-infrared bands, respectively.

- NDWI

The NDWI indicates wetness information, specifically related to the characteristics of water-related components, including soil, plants, and built-up areas [110]. This index offers valuable insights into detecting watery areas, measuring soil moisture levels, and monitoring water changes in the studied areas. Positive NDWI values typically highlight moist and watery regions, whereas negative values suggest dry and water-deprived areas. This information is instrumental in monitoring changes in water resources, managing water resources, and planning water resource utilization. The NDWI was calculated based on Equation (3):

$$\mathrm{NDWI} = \frac{\rho_{\mathrm{Green}} - \rho_{\mathrm{Red}}}{\rho_{\mathrm{Green}} + \rho_{\mathrm{Red}}} \quad (3)$$

where ρ_{Green} and ρ_{Red} represent the green and red bands, respectively.

After generating maps for these spectral indices, these maps were classified based on the provided information in Table 1. Subsequently, the area of each class and the trend of changes in the study period were calculated and compared with each other.

Table 1. Defined ranges for classifying maps of surface biophysical characteristics.

Class	NDVI Range	NDBI Range	NDWI Range
Very low	NDVI < 0	NDBI < −0.10	NDWI < −0.10
Low	0 < NDVI < 0.15	−0.10 < NDBI < 0.0	−0.10 < NDWI < 0.0
High	0.15 < NDVI < 0.30	0.0 < NDBI < 0.10	0.0 < NDWI < 0.10
Very high	NDVI > 0.30	NDBI > 0.10	NDWI > 0.10

3.2.3. Land Surface Temperature (LST)

In this study, the LST maps of Kerman and Zahedan cities were extracted using the Landsat provisional surface temperature (LPST) product. The average of this product for the months of May, June, July, and August each year was used as the LST map. The use of the average from the four warm months aimed to reduce and normalize the impact of climatic and environmental conditions on LST during the satellite's overpass time. After obtaining the LST map: (1) the average LST was calculated for the study area, and its comparison was conducted with land cover classes in different years; (2) the map of LST changes was prepared for the study period using the difference operator, and the spatial and temporal variations in LST were evaluated; (3) the correlation coefficient between surface biophysical characteristics and LST was calculated for different years and compared; (4) the classified map of LST in Kerman and Zahedan cities was generated with classes such as very low LST (LST < 32 °C), low LST (32 °C < LST < 37 °C), moderate LST (37 °C < LST < 42 °C), high LST (42 °C < LST < 47 °C), and very high LST (LST > 47 °C); and (5) subsequently, the area of LST classes was calculated for different years, and the trend of changes during the

study period was evaluated. ArcMap 10.3 software was used for classifying LST maps and calculating the area of LST classes.

- Prediction of future LST map

The details of the method for predicting LST were presented in Firozjaei et al. [31], Nadizadeh Shorabeh et al. [30], and Kiavarz et al. [29]. To predict the LST, the trends in land cover changes and the resulting changes in LST over the past 37 years have been utilized. The extent of LST changes for each type of land cover change was examined at different time intervals. Accordingly, the average LST change resulting from each type of land cover change was calculated. Subsequently, using the predicted land cover change map for the future and the matrix of average LST changes resulting from land cover change, the map of future LST changes was generated. By combining the map of LST changes for the time period 2023–2045 with the LST map for the year 2023, the LST map for the year 2045 was produced.

3.2.4. Surface Urban Cool Island Intensity (SUCII)

Initially, to normalize the LST values for different years concerning changes in climatic and seasonal conditions, the LST values for each pixel were subtracted from the average LST value for areas with NDVI > 0.6 [2,111]. Regions with NDVI > 0.6 in the study area represent pixels containing vegetation cover with full canopy. The surface temperature of these pixels is close to the air temperature, and it can be used to normalize climatic and seasonal conditions. The normalized LST maps were then obtained. In this study, to calculate the SUCII in each geographical location, the difference between the normalized LST in each pixel and the average normalized LST for the study area in different years was calculated using Equation (4):

$$SUCII_{Pixel} = NLST_{Pixel} - \overline{NLST_{study\ area}} \quad (4)$$

where $SUCII_{Pixel}$ represents the urban cold island intensity in each pixel, $NLST_{Pixel}$ represent the normalized surface temperature at the pixel, and $\overline{NLST_{study\ area}}$ represents the average normalized surface temperature for the study area. The SUCII maps and their changes were prepared using ArcMap 10.3 software.

4. Results

4.1. Land Cover

Land cover maps of Kerman and Zahedan cities for different years are presented in Figure 3. The overall accuracy of the generated Kerman (Zahedan) land cover maps for the years 1986, 1994, 2001, 2008, 2015, and 2023 was 91% (92%), 88% (91%), 89% (89%), 87% (89%), 92% (91%), and 91% (92%), respectively. The predicted land cover map overall accuracy of Kerman (Zahedan) city for 2023 relative to land cover map for 2023 obtained from the classification algorithm was 84% (86%), indicating the CA-Markov model's capability of predicting the spatial distribution of land cover for the study area in the future. The dominant land cover in Kerman and Zahedan cities includes built-up and bare lands. The considerable physical growth of built-up areas in these cities was noticeable. The horizontal expansion of Kerman and Zahedan cities in recent years has led to the destruction of natural lands on the city's outskirts. Consequently, the physical growth of the city has transformed a significant amount of green and bare lands into built-up areas. This trend is expected to continue in future years. Given the rising land/house prices, vertical expansion of the city could be argued to minimize the horizontal expansion.

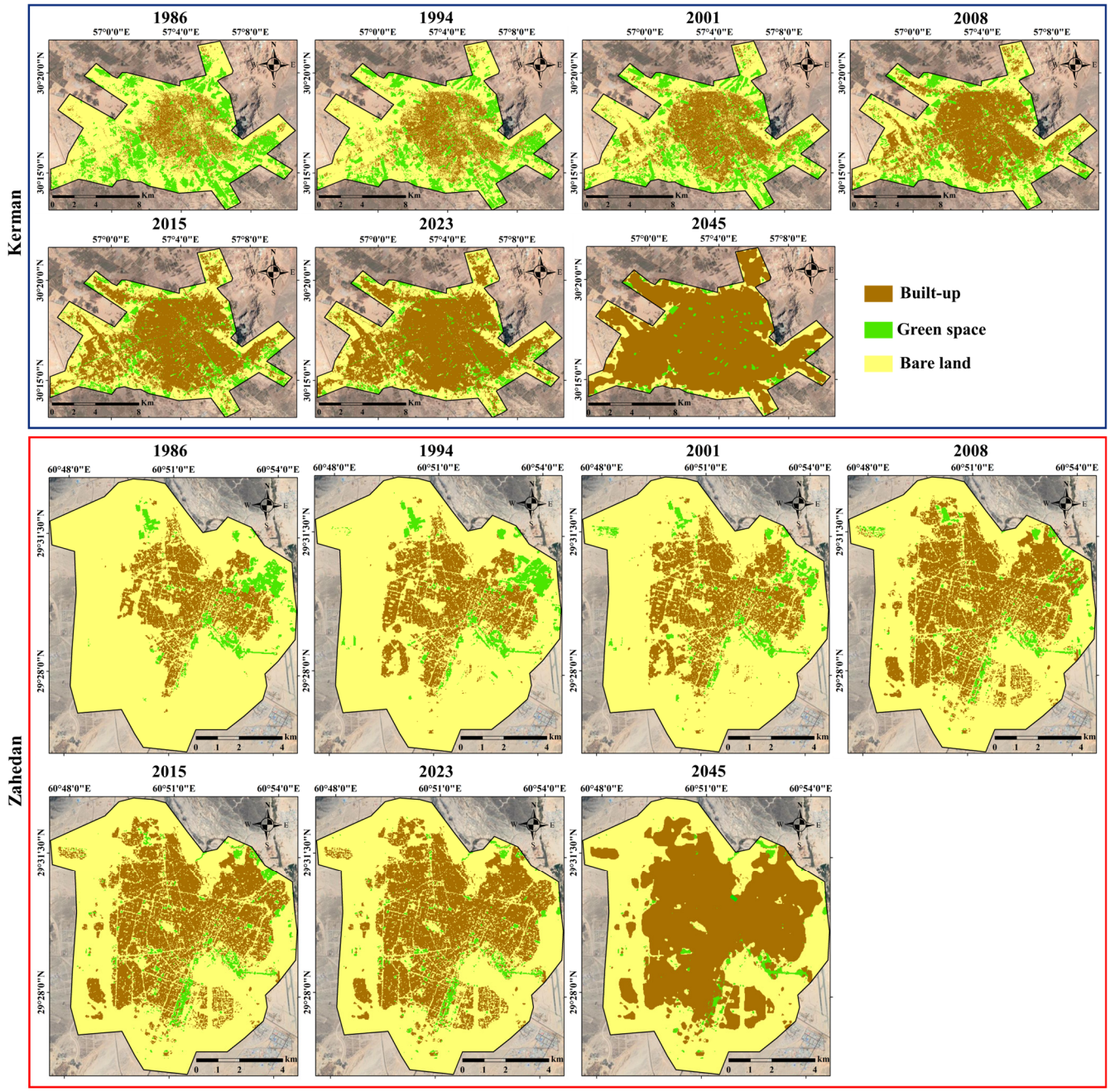

Figure 3. Land cover maps of Kerman and Zahedan cities for different years.

The area percentage of different land cover classes in Kerman and Zahedan cities shows a considerable increase in the built-up areas over the past years. Conversely, the bare lands and green spaces have shown a significant reduction due to conversion into built-up areas (Figure 4). In 1986, the area percentage of built-up, bare, and green spaces in Kerman (Zahedan) city was 15% (15%), 59% (80%), and 26% (5%), respectively. These values reached 57% (36%), 35% (61%), and 8% (3%) in 2023. By 2023, the built-up area of Kerman (Zahedan) city has increased by approximately 272% (138%). The area of bare lands and green spaces in Kerman (Zahedan) city has decreased by about 40% (39%) and 69% (24%), respectively. By 2045, the area percentage of built-up, bare, and green spaces of Kerman (Zahedan) city is expected to be 72% (49%), 24% (49%), and 4% (2%), respectively. In the next 22 years, approximately 11% (12%) and 4% (1%) of bare lands and green spaces in Kerman (Zahedan) city are expected to be converted into built-up areas. The built-up area of Kerman (Zahedan) city is expected to increase by about 15% (13%) by 2045.

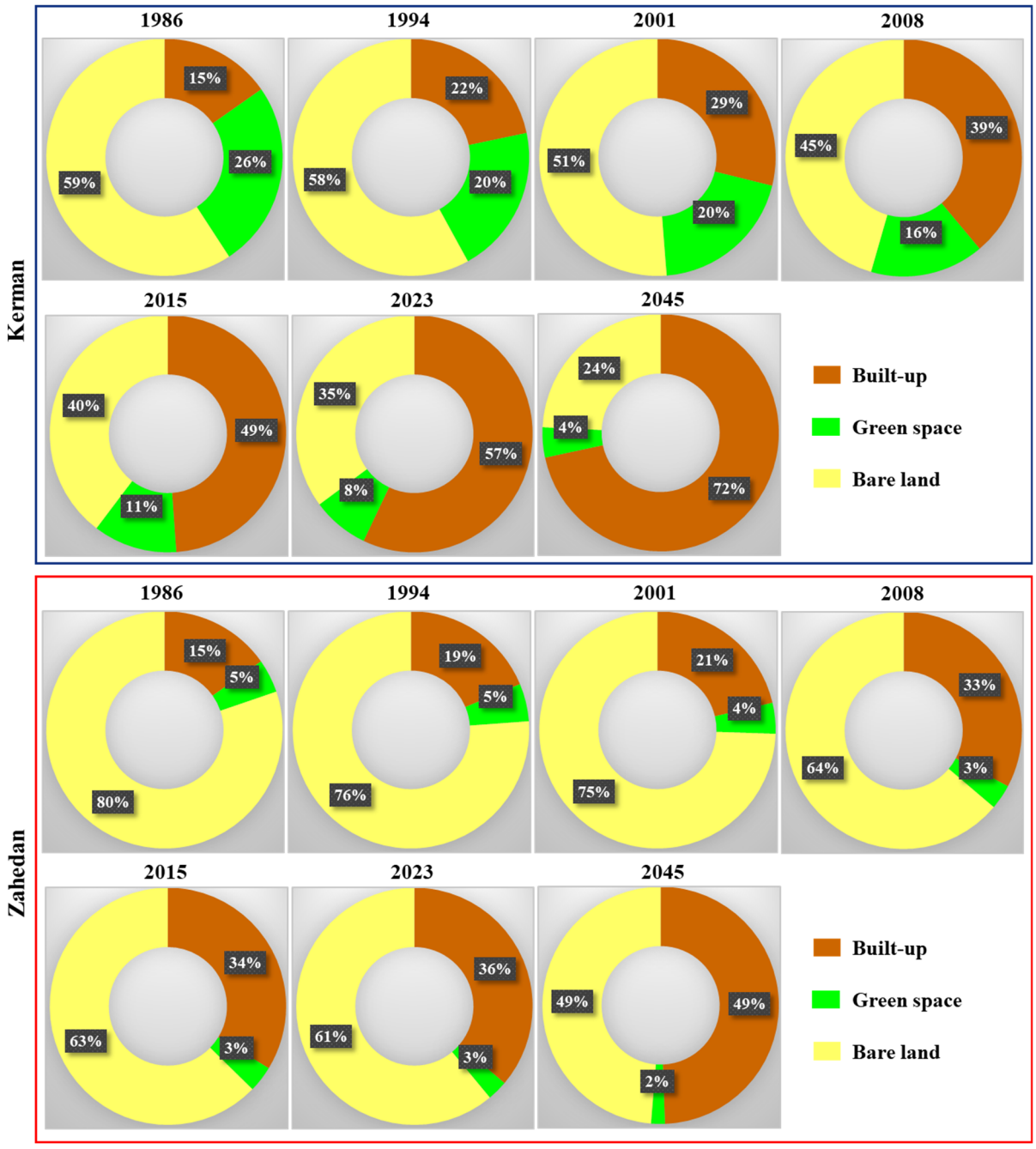

Figure 4. Area percentage of different land cover classes in Kerman and Zahedan cities over the years (%).

4.2. Surface Biophysical Characteristics

Maps of NDBI, NDVI, and NDWI classes for Kerman and Zahedan cities in different years were illustrated in Figure 5. The average values of NDVI, NDBI, and NDWI for Kerman (Zahedan) city have changed from 0.14 (0.10), 0 (0.05), and −0.07 (−0.04) in 1986 to 0.11 (0.08), 0.07 (0.11), and −0.01 (0.0) in 2023, respectively. During this period, the average values of NDBI and NDWI for Kerman (Zahedan) city have increased by 0.07 (0.06) and 0.06 (0.04), respectively, while the average value of NDVI has decreased by 0.03 (0.02). The increase in average NDWI in Kerman and Zahedan cities indicates the warming and drying of the built-up areas from the surrounding barren lands, and a significant portion of these lands has transformed into developed areas in recent years. Additionally, the increase in

the average NDBI index reflects the degree of surface imperviousness, as it increases with the fraction of impervious surfaces in a pixel.

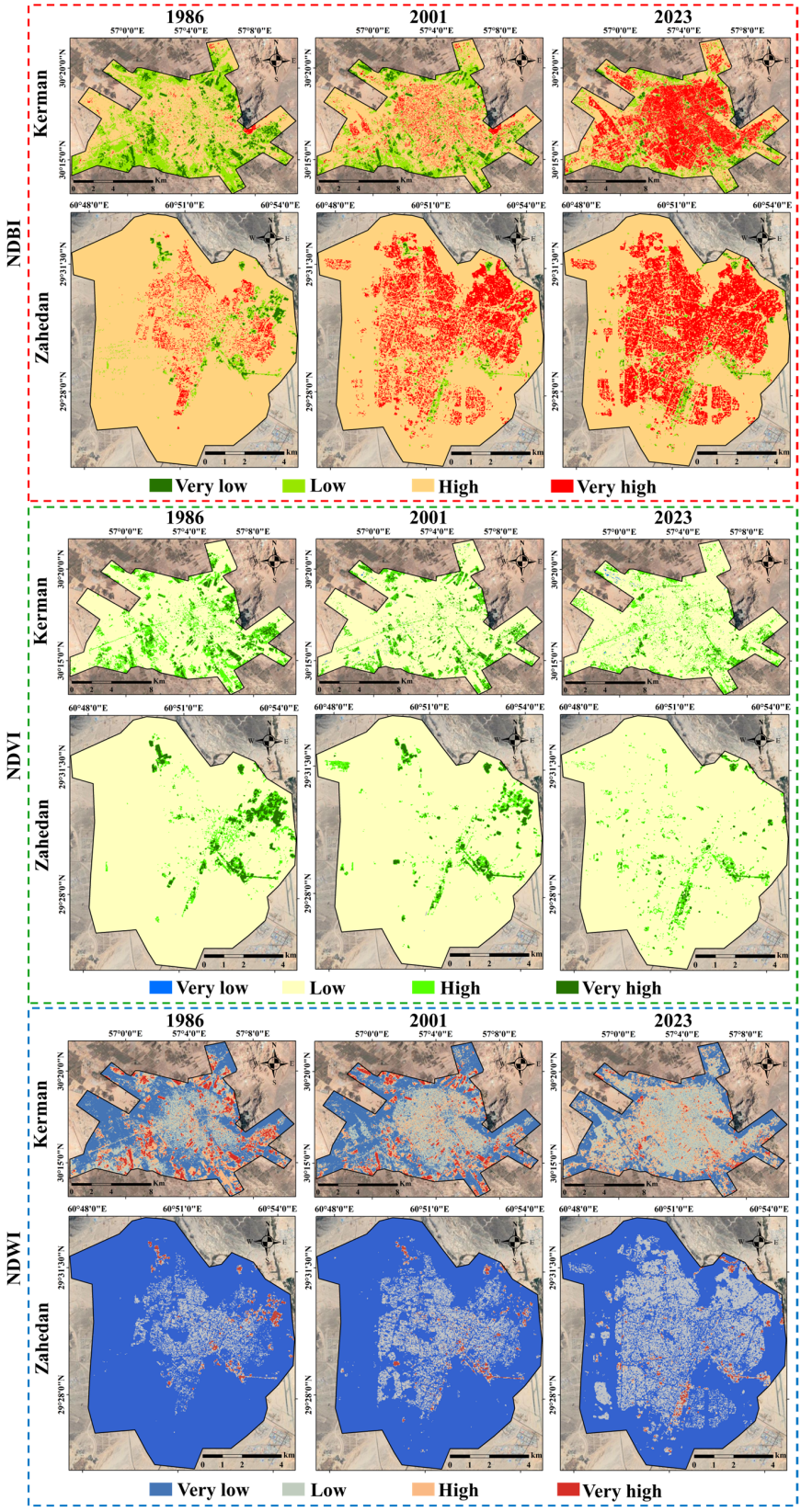

Figure 5. Maps of NDBI, NDVI, and NDWI classes for Kerman and Zahedan cities in different years.

Areas with very high NDBI values were mostly situated in built-up lands. Green spaces were primarily classified in the low and very low NDBI classes, while barren lands were mostly classified in the high NDBI class. The transformation of green and barren lands into built-up areas increases the surface imperviousness; hence, areas with high NDBI have expanded. The NDBI values range between −1 and 1, with an increase in impervious surfaces leading to values closer to 1. The area of the very high NDBI class in Kerman (Zahedan) city has increased significantly from 3.0 km^2 (6.1 km^2) in 1986 to 64.2 km^2 (33.7 km^2) in 2023. Conversely, the areas of high, low, and very low NDBI classes in Kerman (Zahedan) city have decreased noticeably, reaching 82.8 km^2 (78.0 km^2), 21.9 km^2 (3.2 km^2), and 5.1 km^2 (0.8 km^2) in 2023 from 94.9 km^2 (104.3 km^2), 60.2 km^2 (3.8 km^2), and 15.9 km^2 (1.5 km^2) in 1986, indicating a considerable reduction. Most areas with high and very high NDVI were located around the urban periphery. In contrast, areas with low and very low NDVI were positioned within the urban boundary. The areas with high and very high NDVI in Kerman (Zahedan) city have significantly decreased until 2023, with a total reduction of approximately 11 km^2 (2.8 km^2) in this period. In contrast, the total area of low and very low NDVI classes in Kerman (Zahedan) city has increased from 135.2 km^2 (107.0 km^2) in 1987 to 146.2 km^2 (109.9 km^2) in 2023, indicating an expansion of these classes. The growth of built-up areas has led to the destruction of green spaces in Kerman and Zahedan cities. High and very high vegetation cover clusters have disappeared or had their areas significantly reduced. Due to the absence of aquatic lands in Kerman and Zahedan cities, these regions lack a very low vegetation cover class. The area of NDWI classes in Kerman (Zahedan) city, including very low, low, high, and very high, has changed from 82.9 km^2 (101.7 km^2), 43.1 km^2 (11.9 km^2), 32.3 km^2 (0.9 km^2), and 15.8 km^2 (1.3 km^2) in 1987 to 57.2 km^2 (77.1 km^2), 68.4 km^2 (35.7 km^2), 42.5 km^2 (1.4 km^2) and 5.8 km^2 (1.4 km^2) in 2023, respectively. In this period, the areas of very low and very high NDWI classes have increased, while the low and high classes have decreased. Green spaces were classified in the very high NDWI class; however, due to the high surface dryness of barren lands caused by high solar energy receipt, barren lands have fallen into the very low NDWI class in these cities. The NDWI class of built-up lands in these cities was generally low and high. Therefore, over the past 37 years, with the transformation of a considerable area from barren lands to built-up areas, areas with low and high NDWI classes in these cities have increased.

4.3. Maps of Land Surface Temperature (LST)

Classified LST maps for Kerman and Zahedan cities for various years are displayed in Figure 6. Areas with high and very high LST in Kerman and Zahedan cities were located outside the built-up land area. Pixels within urban areas are usually heterogeneous, including green spaces, shadows, and moisture, resulting in lower LST compared with the peripheral areas with barren land cover. The average (standard deviation) LSTs of built-up land, green spaces, and barren land of Kerman city in 1986 were 47.9 °C (1.7 °C), 46.9 °C (3.3 °C), and 50.1 °C (2.5 °C), respectively. These values have decreased in 2023 to 44.1 °C (3.5 °C), 43.1 °C (4.3 °C), and 49.5 °C (3.2 °C), respectively. For Zahedan city, the average (standard deviation) LSTs of built-up land, green spaces, and barren land in 1986 were 45.2 °C (1.3 °C), 44.4 °C (2.5 °C), and 49.5 °C (2.0 °C), respectively. These values have decreased in 2023 to 43.3 °C (2.3 °C), 44.6 °C (2.9 °C), and 49.1 °C (3.2 °C), respectively. The average LST of Kerman (Zahedan) city has decreased from 49.1 °C (48.6 °C) in 1986 to 44.6 °C (45.1 °C) in 2023. The LST of built-up land was lower than that of barren land, and as a result, the average LST of the study area has decreased due to the physical growth of the city and the reduction of barren land.

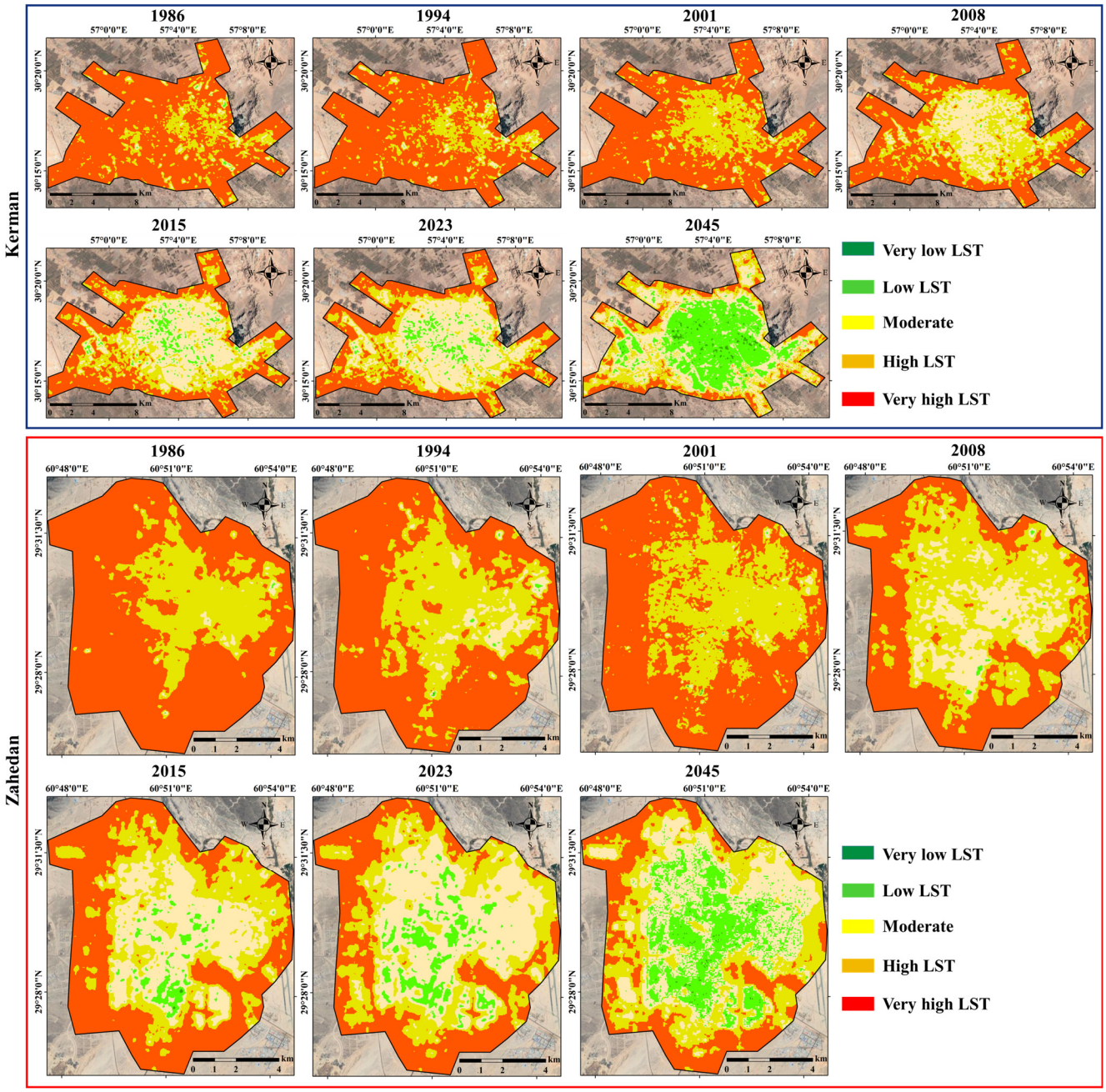

Figure 6. Classified maps of LST for Kerman and Zahedan cities in different years.

In the years 1987, 1994, and 2001, most of the built-up land areas were classified into the high and very high LST classes, mainly due to the presence of pixels with a combination of developed and barren land cover in urban areas. However, with the increasing density of built-up land within a pixel in the years 2008, 2015, and 2023, more built-up land areas have fallen into the moderate LST class. Over the past years, the expansion of built-up land areas in the outskirts has led to the extension of areas with moderate and low LST. This expansion trend is expected to continue until 2045, as visible on the predicted LST map of Kerman and Zahedan cities. The most significant reduction in the area of LST classes in Kerman (Zahedan) city was related to the very high LST class, which has decreased from 138.9 km^2 (84.9 km^2) in 1986 to 58.49 km^2 (34.4 km^2) in 2023. Additionally, the area of low, moderate, and high LST classes has increased from 0.33 km^2 (0.03 km^2), 3.5 km^2 (0.9 km^2) and 31.21 km^2 (30.1 km^2) in 1986 to 8.0 km^2 (7.9 km^2), 62.8 km^2 (39.8 km^2), and 44.7 km^2 (33.6 km^2) in 2023. Over the study period, Kerman does not have a very low

LST class. In the past 37 years, the total area of high and very high LST classes in Kerman and Zahedan has significantly decreased. This value is expected to reach 63 km^2 and 19.8 km^2 in 2045, respectively. The total area of moderate, low, and very low LST classes in Kerman (Zahedan) city in 1986, 2023, and 2045 was calculated as 4 km^2 (30.9 km^2), 70 km^2 (81.3 km^2), and 110 km^2 (91.4 km^2), respectively.

4.4. Land Cover, Surface Biophysical Properties, and LST Changes

Maps of land cover, LST, NDVI, NDBI, and NDWI changes for Kerman and Zahedan cities are shown in Figure 7. The transformation of green and bare land into built-up areas in Kerman (Zahedan) city has amounted to 20.1 km^2 (2.2 km^2) and 52.5 km^2 (22.1 km^2), respectively, between 1986 and 2023. Land cover changes have resulted in alterations in surface biophysical properties. Over the study period, LST for Kerman (Zahedan) city has fluctuated between −18 °C (−16 °C) and 15 °C (14 °C). The temperature of built-up areas has generally decreased. The highest increase (decrease) in NDVI, NDBI, and NDWI in Kerman city was 0.65 (−0.69), 0.62 (−0.49), and 0.67 (−0.54), respectively; these values for Zahedan city were 0.63 (−0.62), 0.51 (−0.42), and 0.47 (−0.50), respectively. Over the past 37 years, the highest average increase in LST of Kerman (Zahedan) city was associated with the conversion of green areas to bare and built-up land, amounting to 5.5 °C (4.3 °C) and 1.5 °C (1.7 °C), respectively. On average, the transformation of bare land to built-up areas of Kerman (Zahedan) city has resulted in a 4.6 °C (3.8 °C) reduction in LST in Kerman. Additionally, the LST of areas consistently classified as built-up overall years has decreased by 2.7 °C (2.4 °C).

The highest average change in NDVI for Kerman (Zahedan) city, with a value of 0.13 (0.20), was related to the conversion of bare land to green areas. The transformation of bare and green areas into built-up land in Kerman (Zahedan) city has led to a decrease in NDVI by 0.03 (0.02) and 0.13 (0.18), respectively. Moreover, the highest average change in NDBI of Kerman (Zahedan) city, amounting to 0.19 (0.14), was associated with the conversion of green areas to built-up land. The transformation of bare land to built-up areas in Kerman (Zahedan) city has, on average, increased NDBI by 0.1 (0.06). The NDBI value for areas consistently classified as built-up in Kerman (Zahedan) city in both 1987 and 2023 has also increased by 0.06 (0.05), indicating an increase in the built-up land density in these areas. The most significant average change in NDWI was observed in the conversion of bare land to green areas (0.17 for Kerman city and 0.12 for Zahedan city), with an average increase in NDWI of 0.1 and 0.05 resulting from the transformation of bare land to built-up areas in Kerman and Zahedan cities, respectively. The results demonstrate that land cover changes significantly influence surface biophysical characteristics.

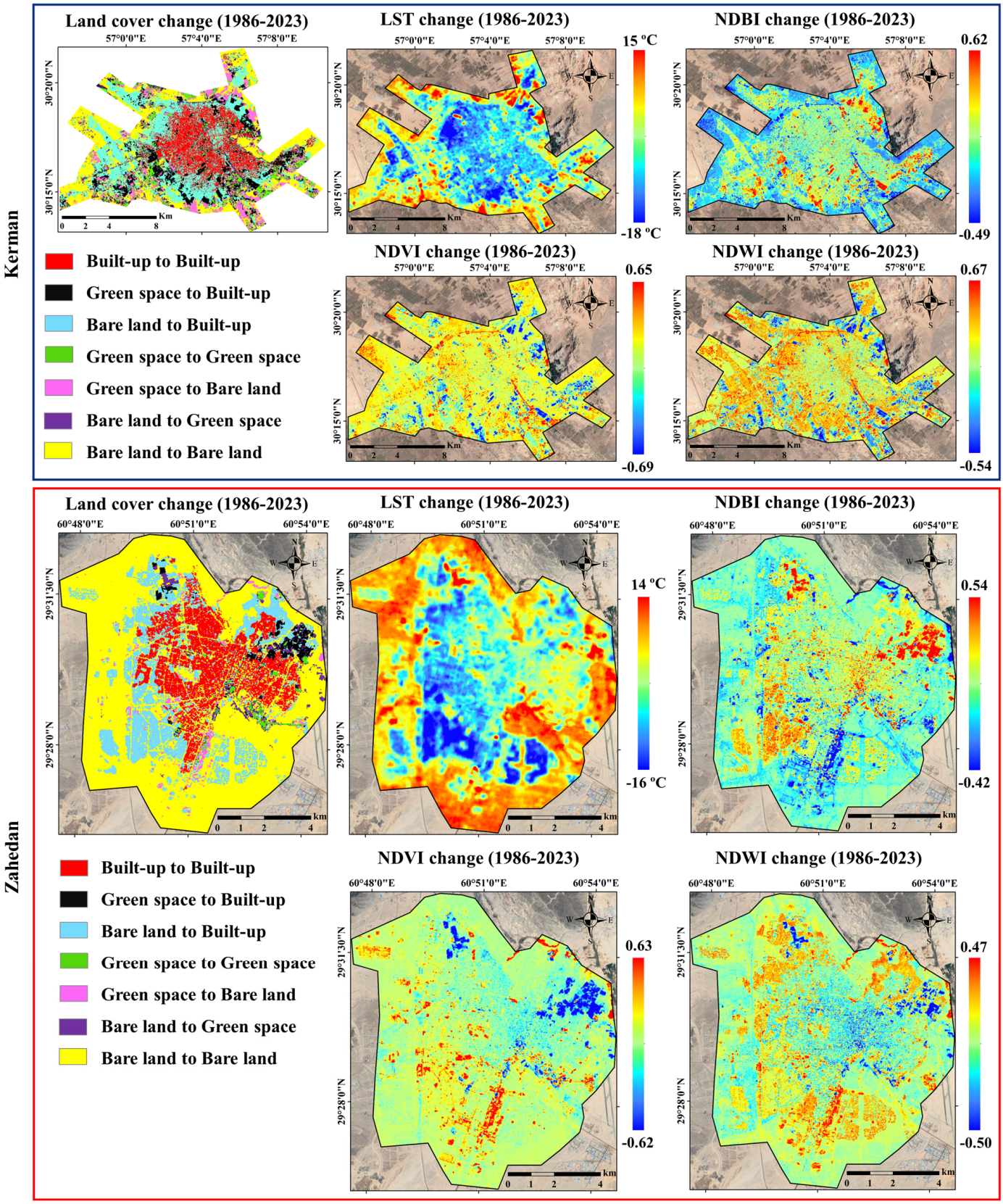

Figure 7. Maps of changes in the LST, NDVI, NDBI, and NDWI of Kerman and Zahedan cities for the study period.

4.5. Maps of Surface Urban Cool Island Intensity (SUCII)

The SUCII maps for the Kerman and Zahedan cities for various years are illustrated in Figure 8. The trend in the SUCII for these cities from 1986 to 2023 shows an increasing pattern, mainly attributed to the conversion of barren lands into built-up areas. The highest and lowest SUCII values were generally located inside and around the urban boundary, respectively. The transformation of barren lands into built-up areas has led to a significant increase in SUCII in these regions. However, in some parts of this area, the conversion of green spaces into built-up areas has resulted in decreased SUCII. Moreover, the SUCII of areas converted from barren lands to green spaces have significantly increased. The trend of decreasing areas with medium and high SUCII in Kerman was expected to continue until 2045. The estimated SUCII values for Kerman in 1986, 1994, 2001, 2008, 2015, and 2023 were −0.3 °C, −0.8 °C, −1.4 °C, −1.9 °C, −2.6, and −3.2 °C, respectively. These values for Zahedan were 0.9 °C, 0.4 °C, −0.5 °C, −1.5 °C, −2.5 °C, and −3.4 °C, respectively. The SUCIIs for Kerman and Zahedan indicate a decreasing trend, suggesting a cooling effect in these urban areas. The results show that the SUCII in Kerman (Zahedan) has increased by 2.9 (4.3) °C over the past 36 years. The SUCII values in Kerman and Zahedan are expected to reach −4.5 and −4.9 °C in 2045, indicating an increase in SUCII in the future. The determination coefficients between the built-up area, population, and SUCII for Kerman (Zahedan) were 0.91 (0.89) and 0.83 (0.84), respectively. The relationship between the built-up area, population, and SUCII in these cities was direct; in other words, as the built-up area and population of Kerman increased, the SUCII in these cities increased.

The area percentage of SUCII classes in Kerman and Zahedan cities is depicted in Figure 9. In Kerman (Zahedan), the areas percentage of regions classified as non-SUCII, low SUCII, medium SUCII, and high SUCII in 1986 were 50% (76%), 23% (13%), 18% (10%), and 9% (1%), respectively. These values reached 25% (29%), 28% (21%), 24% (20%), and 23% (30%) in 2023, respectively. The area percentage of non-SUCII regions in Kerman (Zahedan) decreased by 25% (47%) during this period, while the areas of low SUCII, medium SUCII, and high SUCII increased by 5% (8%), 6% (10%), and 14% (29%), respectively. Until 2015, the largest area percentage belonged to the non-SUCII class in Kerman and Zahedan, but in 2023, the area percentage of the low SUCII class in Kerman and high SUCII class in Zahedan exceeded that of the non-SUCII class. The area percentage of non-SUCII class in Karman (Zahedan) is expected to decrease to 18% (18%) in 2045 compared with 2023. Additionally, the areas percentage of medium SUCII and high SUCII classes in Kerman are expected to increase to 26% and 30%, respectively, compared with 2023. These values were 18% and 38% for Zahedan, respectively.

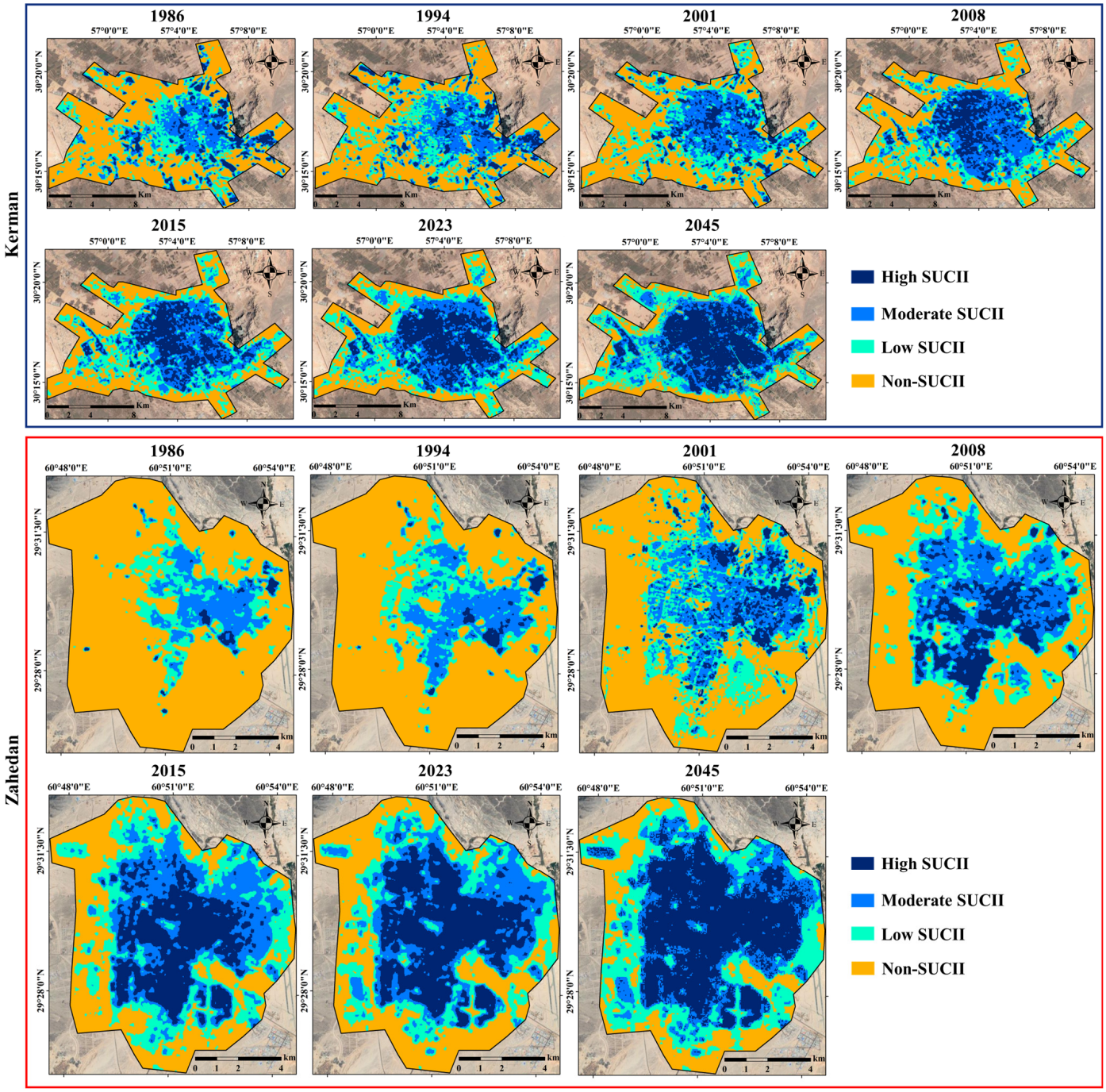

Figure 8. SUCII maps for Kerman and Zahedan cities for different years.

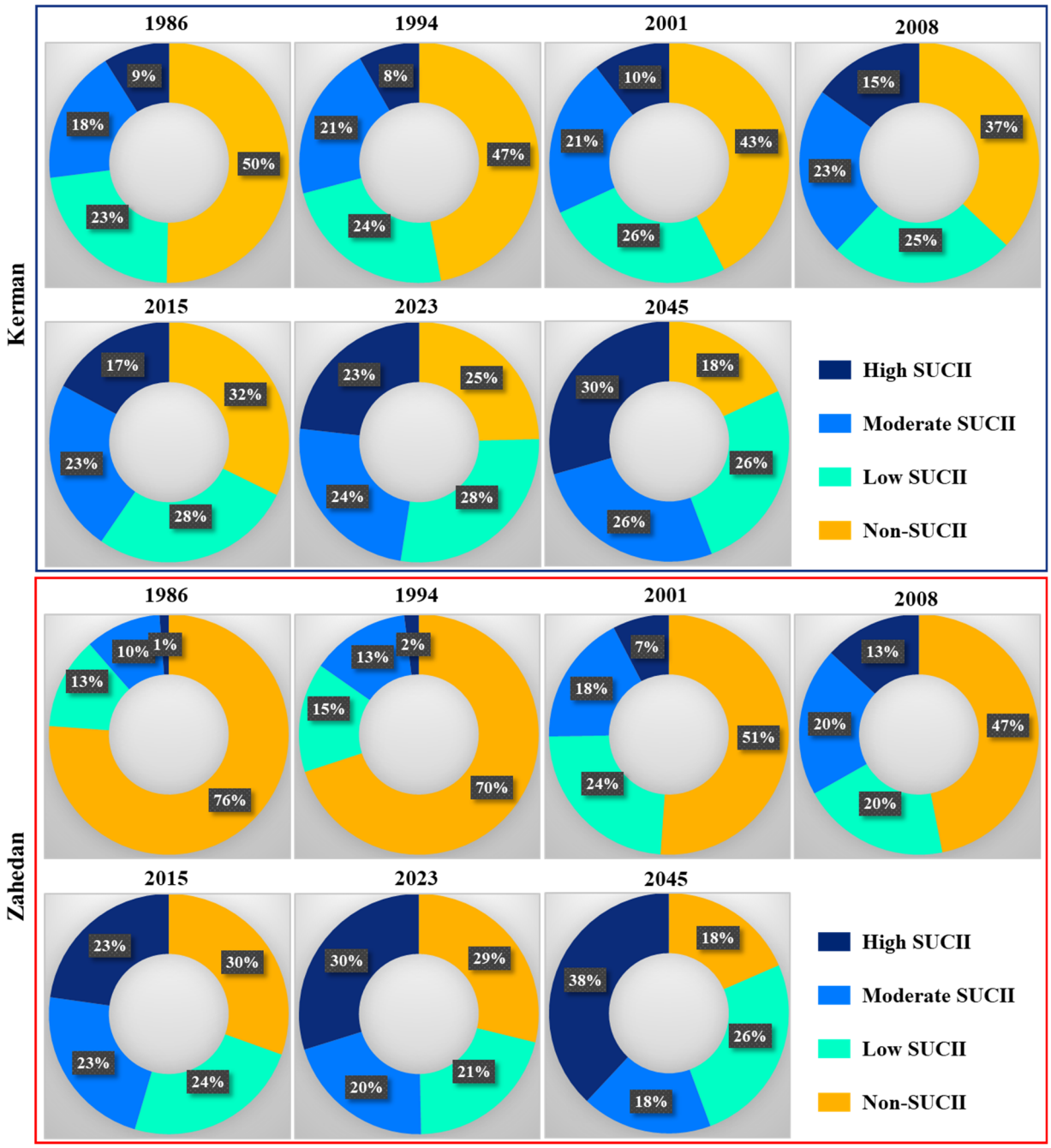

Figure 9. Area percentage of different SUCII classes in Kerman and Zahedan cities for various years.

5. Discussion

Our finding reveals that the built-up area of Kerman (Zahedan) city has increased by approximately 272% (138%) within 1986–2023. The area of bare lands and green spaces in this city has decreased by about 40% (39%) and 69% (24%), respectively (Figures 3 and 4). In the same period, the study area was physically expanded largely due to economic development rooted in industrial activities such as mining, rural–urban migration, long-term droughts and other climate change-born impacts, and lack of proper policies. The city has expanded outward, with new housing and commercial developments extending into the surrounding desert areas. Kerman and Zahedan are situated in a hot and arid climate with large surrounding affordable barren lands available for development not in favor of vertical expansion, i.e., a large share of the constructed buildings are less than three-story buildings expanding around the city outskirts and suburban areas. Thus, vertical

expansion is insignificant to be included in the urban expansion simulation. Over the past four decades in Kerman (Zahedan) city, more than 52.5 km^2 (21.8 km^2) of bare lands have been transformed into built-up areas. This result is consistent with findings from other studies conducted in arid regions [112–116]. Wang et al. [112] demonstrated that bare land in the Shiyang River Basin (SRB), primarily located in the Tengger Desert, Badain Jaran, and the surrounding Gobi area, has been continuously decreasing due to urban physical growth from 1987 to 2017.

Our simulation results indicate that the physical growth of Kerman and Zahedan cities and the reduction of barren lands and green spaces are expected to continue in the future, as shown in Figures 3 and 4. Mansour et al. [117] conducted a study examining the physical growth of the city of Ibri in Oman, which has a climate similar to Kerman. The results of this study showed that changes in land use and land cover (LULC) across the city were rapid between 2010 and 2020, converting desert, bare land, and vegetation into urban areas. Projections indicate that the area of land conversion from desert to urban regions will reach 56.6 km^2 in the next two decades and 77.5 km^2 by 2045. This is in line with the projected population and urban growth for Asian, African, and South American cities, possibly jeopardizing their pathways towards sustainable development goals [44,81,94]. One crucial example of such consequences is the alteration of LST [16,46]. For instance, in humid and tropical climate zones, the replacement of natural permeable surfaces with impermeable surfaces reduces the amount of greenery and surface roughness, disrupting the energy balance of the natural surfaces. This results in an increase in LST while creating and intensifying the SUHI effect [16,31,41,75]. Previous studies have shown that the physical growth of cities in humid climates leads to an increase in the area of the high LST class and, consequently, an increase in the intensity of the heat island effect. Typically, the land cover around these cities includes agricultural land, green spaces, and water surfaces which, due to high vegetation and moisture, have lower LSTs. Urban expansion transforms these areas into built-up and impermeable land, leading to a considerable increase in LST. However, it is different in the arid regions surrounding cities as the land cover consists of barren lands (Figure 3). These areas have higher LST during the day compared with built-up areas (Figure 6) due to factors such as the lack of shade, low surface roughness, high aridity, and low latent and sensible heat fluxes. However, in urban environments, green spaces, water bodies, and building shadows contribute to cooling effects [36,50–52], which is also evident in the case study as the average NDWI has risen due to urban expansion (Figures 5 and 7). It should be noted that the emissivity coefficient of built-up lands is higher than that of barren lands [41,71]. The higher emissivity coefficient results in the absorption of a higher amount of solar energy, a significant portion of which is released with a slight delay during the night. In cases where the absorption and retention of solar energy at the surface of barren lands are low, the LST rises quickly. Another explanation for why bare soil has higher LST values compared with urban surfaces is the concentration of heat, low vegetation cover, low relative humidity, and surface dryness in the upper layers of sandy soil [118]. During the summer, sandy soil has lower water content and faster drainage, which leads to higher LST. Bare soil in this region is characterized by sandy soil with lower water retention capacity and lower thermal inertia [119]. In contrast, other types of soil, such as clay soil used for planting, have higher water retention capacities. Therefore, the higher the water content in the soil, the slower the drainage rate, resulting in a decrease in the LST. This surface temperature difference confirms that the SUHI effect has an inverse effect and an overall negative impact on the urban environment in arid regions. These findings align with the studies of Abulibdeh [119], Parvez et al. [120], and Rida et al. [118]. Abulibdeh [119] demonstrated that the average surface temperature of bare land areas was approximately 2 °C higher than that of urban areas in eight arid and semi-arid Gulf region cities. They demonstrated that spatiotemporal variations in LST in arid climates exhibit an inverse effect due to the nature of urban fringe areas, which possess soil with desert-like characteristics. As a result, cities located in dry environments are cooler during the day than suburban areas and vice versa during the night. The physical

growth of the city, leading to the replacement of these areas with built-up areas, results in a reduction in LST (Figures 6 and 7). Accordingly, the SUCII in Kerman and Zahedan has decreased in recent years due to the growth of built-up areas and the reduction of barren lands (Figures 8 and 9). Previous studies have also shown that cities such as Jeddah [121], Isfahan [51], Dubai [122], Erbil [50], Mash'abei-Sadeh [123], Bengaluru [52], Tehran [36], Kuwait [47], Ulaanbaatar [124], and arid cities in the United States [125], located in dry environments, are cooler than suburban areas in the day time.

The findings of this study indicate that the physical growth of cities in arid and semi-arid regions, considering the climatic characteristics of these areas, can have positive effects on the thermal quality of the urban environment. For example, while urban growth in humid areas typically leads to an increase in the UHI effect, in dry regions, the reduction of barren surfaces and the increase in construction can result in lower surface temperatures during the day. This suggests that urban development policies in arid areas should focus on reducing barren surfaces and enhancing green and blue infrastructure, such as parks and urban green spaces. Urban planners should leverage these findings and prioritize development policies that promote climate sustainability in cities, such as using highly reflective building materials and creating more green spaces. These findings can assist in the development of climate-resilient urban areas. Policy makers can design appropriate strategies to address extreme climatic phenomena, such as heatwaves, using projected data on urban growth and its impact on surface temperatures. Particularly in areas with access to barren lands, planning for the optimal use of these lands through the creation of green infrastructure and sustainable buildings can help mitigate urban heat effects. Additionally, developing policies aimed at increasing green spaces and reducing impervious surfaces can help alleviate the impacts of UHI in arid regions.

6. Conclusions

Forecasting future urban development arising from population growth and socioeconomic activities is fundamental for sustainable urban planning. Such insights should be used to study the cascading changes in the thermal quality of the urban environment, which is crucial for urban planning, improving the quality of urban ecosystems, and ultimately enhancing the quality of human life. The type and extent of the impact of urban growth on changes in the thermal quality of the urban environment can vary depending on the climatic conditions in which a city is located. Therefore, understanding the differences in how urban growth affects changes in the thermal quality of the urban environment in regions with different climates is vital for the development of effective urban development and sustainable urban environments. In summary, previous studies have predominantly focused on SUHIs rather than SUCIs. Additionally, a notable finding is that 35% of global big cities are located in drylands. Most research has concentrated on the spatial and temporal changes of SUCIs in drylands in the past, and there is a gap in predicting the future spatiotemporal changes in SUCIs for cities in dryland areas. The lack of attention on forecasting SUCI dynamics in these regions presents an opportunity for future research. This study showcased how to forecast the spatiotemporal dynamics of SUCIs in response to the urbanization process in drylands using geographical data and models. The area of built-up land in Kerman (Zahedan) city located in a dry region increased by approximately 272% (138%), followed by a decrease in bare lands and green spaces by about 40% (39%) and 69% (24%), respectively, in the studied period. The conversion of bare land to built-up land has led to an average decrease of 4.6 °C (3.8 °C) in LST in this city. The most notable land conversion in Kerman and Zahedan cities has been the conversion from bare land to built-up land. Consequently, the area of high and very high temperature classes in Kerman and Zahedan cities has significantly decreased. The SUCII of Kerman (Zahedan) city has decreased from −0.3 °C (0.9 °C) in 1987 to −3.2 °C (−3.4 °C) in 2023. By 2045, approximately 31% (19%) of its bare land is expected to be converted to built-up land, resulting in a decrease in LST and an increase in SUCII. The physical growth of cities in arid and semi-arid regions improves the thermal quality of the urban environment, which should be

further supplemented by adding green and blue infrastructure where possible. Therefore, the physical growth of cities located in hot and arid regions, despite those located in humid climates, can mitigate the heat comfort concerns. Hence, urban development plans embracing climate-friendly, climate-neutral, green, and environmentally friendly urban planning frameworks should be prioritized in arid regions. The methodical approach, choice of data, presented findings, and discussions can be inspirational for a broader community of researchers, urban planners, and decision makers.

7. Limitations and Future Directions

The present study has provided valuable insights into the relationship between LST, SUCIs, and land cover in the study area. However, several limitations need to be acknowledged. First, CA-Markov models, while useful for land cover change prediction, have limitations. They assume static transition probabilities, ignoring dynamic factors influencing land cover change. Additionally, these models neglect crucial driving forces and oversimplify spatial patterns, leading to less accurate predictions. Second, the study focused on daytime LSTs during the summer season, limiting the understanding of SUCI dynamics throughout the year. Incorporating nighttime LSTs and data from different seasons would provide a more comprehensive picture of SUCI effects. Third, the spatial resolution of satellite imagery might limit the ability to capture fine-scale variations in LST within urban areas, particularly in densely built-up regions. Higher-resolution data or ground-based measurements could address this limitation. Fourth, the accuracy of LST retrieval can be influenced by factors such as atmospheric conditions, thermal anisotropy, incomplete sampling, and land surface emissivity, which could introduce uncertainties in the results. In this study, the impact of future climate changes on the prediction of surface temperature changes was not included as such data are not available and must be simulated using projected climate data, e.g., temperature, moisture, and land cover/use. Hence, one conclusion of this study is to simulate future LST data so that urban planners and decision makers can investigate how to plan for heatwaves in the future and implement climate-friendly measures.

Future research directions include:

Land cover change prediction improvement: To enhance predictive capabilities, future research should focus on integrating dynamic factors, incorporating socioeconomic and environmental variables, and exploring more sophisticated spatial modeling techniques. Hybrid models combining CA-Markov with machine learning or agent-based modeling can provide more robust and realistic land cover change projections.

Spatial and temporal expansion: Extending the study to cover a larger geographical area and longer time periods to identify regional patterns and trends in SUCI development.

High-resolution analysis: Utilizing higher-resolution satellite imagery and ground-based measurements to investigate intra-urban variations in LST and their relationship with land cover/use, urban morphology, and local climate zones (LCZs). Also, future studies should combine low-resolution geostationary satellites (e.g., GOES) with high-resolution polar-orbiting satellites (e.g., Landsat, MODIS) to address the influence of local time and viewing–illuminating geometry on LST measurements. This combination would improve both temporal and spatial coverage, providing a better understanding of LST variations. Additionally, exploring LST reconstruction methods, such as spatiotemporal fusion and machine learning techniques, can fill data gaps and enhance accuracy. Incorporating atmospheric correction models and improving emissivity estimations could also reduce uncertainties related to thermal anisotropy and atmospheric conditions.

Nighttime UHI: Analyzing nighttime LSTs to understand the diurnal cycle of SUCIs and its impact on human comfort.

Seasonal variations: Investigating the seasonal dynamics of SUCIs and their relationship with meteorological factors.

Urban planning and mitigation strategies: Understanding the SUCII is crucial for effective urban planning and development. By strategically incorporating green infrastruc-

ture, such as parks, green roofs, and urban forests, cities can mitigate the urban heat island effect and enhance livability. Additionally, careful selection of building materials with high reflectivity can reduce heat absorption. Furthermore, SUCII studies can inform land use planning decisions, guiding the placement of residential and commercial areas to optimize thermal comfort. By addressing SUCII, cities can improve public health, reduce energy consumption, and create more sustainable urban environments.

Integration of socioeconomic factors: Incorporating socio-economic variables is important for understanding the vulnerability of different population groups to SUHI.

Additionally, the challenges associated with using satellite-derived LSTs in urban areas should be further explored. This includes the development of advanced techniques for estimating land surface emissivity and correcting for atmospheric effects. Moreover, future research should focus on understanding and modeling thermal anisotropy in urban environments to improve the accuracy of LST-based studies. By addressing these limitations and pursuing the proposed research directions, a deeper understanding of SUHIs and SUCIs and their impacts can be achieved, ultimately informing effective urban planning and mitigation strategies.

Author Contributions: Conceptualization, M.K.F.; methodology, M.K.F. and N.M.; software, M.K.F. and N.M.; validation, M.K.F. and N.M.; formal analysis, M.K.F. and N.M.; investigation, M.K.F., N.M., S.F. and J.J.A.; resources, M.K.F. and N.M.; data curation, M.K.F. and N.M.; writing—original draft preparation, M.K.F., N.M. and S.F.; writing—review and editing, S.F. and J.J.A.; visualization, M.K.F., N.M., S.F. and J.J.A. All authors have read and agreed to the published version of the manuscript.

Funding: This research received no external funding.

Data Availability Statement: The raw data supporting the conclusions of this article will be made available by the authors on request.

Conflicts of Interest: The authors declare no conflicts of interest.

References

1. Li, H.; Zhou, Y.; Li, X.; Meng, L.; Wang, X.; Wu, S.; Sodoudi, S. A new method to quantify surface urban heat island intensity. *Sci. Total Environ.* **2018**, *624*, 262–272. [CrossRef] [PubMed]
2. Mijani, N.; Firozjaei, M.K.; Mijani, M.; Khodabakhshi, A.; Qureshi, S.; Arsanjani, J.J.; Alavipanah, S.K. Exploring the effect of COVID-19 pandemic lockdowns on urban cooling: A tale of three cities. *Adv. Space Res.* **2023**, *71*, 1017–1033. [CrossRef] [PubMed]
3. Santamouris, M.; Kolokotsa, D. On the impact of urban overheating and extreme climatic conditions on housing, energy, comfort and environmental quality of vulnerable population in Europe. *Energy Build.* **2015**, *98*, 125–133. [CrossRef]
4. Huong, H.T.L.; Pathirana, A. Urbanization and climate change impacts on future urban flooding in Can Tho city, Vietnam. *Hydrol. Earth Syst. Sci.* **2013**, *17*, 379–394. [CrossRef]
5. Hall, P.; Pfeiffer, U. *Urban Future 21: A Global Agenda for Twenty-First Century Cities*; Routledge: London, UK, 2013.
6. Voogt, J.A.; Oke, T.R. Thermal remote sensing of urban climates. *Remote Sens. Environ.* **2003**, *86*, 370–384. [CrossRef]
7. Croce, S.; Vettorato, D. Urban surface uses for climate resilient and sustainable cities: A catalogue of solutions. *Sustain. Cities Soc.* **2021**, *75*, 103313. [CrossRef]
8. Musy, M.; Malys, L.; Morille, B.; Inard, C. The use of SOLENE-microclimat model to assess adaptation strategies at the district scale. *Urban Clim.* **2015**, *14*, 213–223. [CrossRef]
9. Klopp, J.M.; Petretta, D.L. The urban sustainable development goal: Indicators, complexity and the politics of measuring cities. *Cities* **2017**, *63*, 92–97. [CrossRef]
10. Dewan, A.M.; Yamaguchi, Y. Land use and land cover change in Greater Dhaka, Bangladesh: Using remote sensing to promote sustainable urbanization. *Appl. Geogr.* **2009**, *29*, 390–401. [CrossRef]
11. Chow, W.T.; Brazel, A.J. Assessing xeriscaping as a sustainable heat island mitigation approach for a desert city. *Build. Environ.* **2012**, *47*, 170–181. [CrossRef]
12. Xiao, H.; Weng, Q. The impact of land use and land cover changes on land surface temperature in a karst area of China. *J. Environ. Manag.* **2007**, *85*, 245–257. [CrossRef] [PubMed]
13. Zhang, H.; Qi, Z.-F.; Ye, X.-Y.; Cai, Y.-B.; Ma, W.-C.; Chen, M.-N. Analysis of land use/land cover change, population shift, and their effects on spatiotemporal patterns of urban heat islands in metropolitan Shanghai, China. *Appl. Geogr.* **2013**, *44*, 121–133. [CrossRef]
14. Zhu, Z.; Woodcock, C.E. Continuous change detection and classification of land cover using all available Landsat data. *Remote Sens. Environ.* **2014**, *144*, 152–171. [CrossRef]

15. Zhou, X.; Chen, H. Impact of urbanization-related land use land cover changes and urban morphology changes on the urban heat island phenomenon. *Sci. Total Environ.* **2018**, *635*, 1467–1476. [CrossRef] [PubMed]
16. Shorabeh, S.N.; Kakroodi, A.A.; Firozjaei, M.K.; Minaei, F.; Homaee, M. Impact Assessment Modeling of Climatic Conditions on Spatial-temporal Changes in Surface Biophysical Properties Driven by Urban Physical Expansion Using Satellite Images. *Sustain. Cities Soc.* **2022**, *80*, 103757. [CrossRef]
17. Chen, S.; Haase, D.; Qureshi, S.; Firozjaei, M.K. Integrated Land Use and Urban Function Impacts on Land Surface Temperature: Implications on Urban Heat Mitigation in Berlin with Eight-Type Spaces. *Sustain. Cities Soc.* **2022**, *83*, 103944. [CrossRef]
18. Firozjaei, M.K.; Alavipanah, S.K.; Liu, H.; Sedighi, A.; Mijani, N.; Kiavarz, M.; Weng, Q. A PCA–OLS Model for Assessing the Impact of Surface Biophysical Parameters on Land Surface Temperature Variations. *Remote Sens.* **2019**, *11*, 2094. [CrossRef]
19. Cheval, S.; Popa, A.-M.; Șandric, I.; Iojă, I.-C. Exploratory analysis of cooling effect of urban lakes on land surface temperature in Bucharest (Romania) using Landsat imagery. *Urban Clim.* **2020**, *34*, 100696. [CrossRef]
20. Vani, M.; Prasad, P.R.C. Assessment of spatio-temporal changes in land use and land cover, urban sprawl, and land surface temperature in and around Vijayawada city, India. *Environ. Dev. Sustain.* **2020**, *22*, 3079–3095. [CrossRef]
21. Wang, R.; Hou, H.; Murayama, Y.; Derdouri, A. Spatiotemporal analysis of land use/cover patterns and their relationship with land surface temperature in Nanjing, China. *Remote Sens.* **2020**, *12*, 440. [CrossRef]
22. Waseem, S.; Khayyam, U. Loss of vegetative cover and increased land surface temperature: A case study of Islamabad, Pakistan. *J. Clean. Prod.* **2019**, *234*, 972–983. [CrossRef]
23. Li, D.; Stucky, B.J.; Deck, J.; Baiser, B.; Guralnick, R.P. The effect of urbanization on plant phenology depends on regional temperature. *Nat. Ecol. Evol.* **2019**, *3*, 1661–1667. [CrossRef] [PubMed]
24. Qiu, T.; Song, C.; Zhang, Y.; Liu, H.; Vose, J.M. Urbanization and climate change jointly shift land surface phenology in the northern mid-latitude large cities. *Remote Sens. Environ.* **2020**, *236*, 111477. [CrossRef]
25. Zhang, L.; Yang, L.; Zohner, C.M.; Crowther, T.W.; Li, M.; Shen, F.; Guo, M.; Qin, J.; Yao, L.; Zhou, C. Direct and indirect impacts of urbanization on vegetation growth across the world's cities. *Sci. Adv.* **2022**, *8*, eabo0095. [CrossRef] [PubMed]
26. Tayyebi, A.; Shafizadeh-Moghadam, H.; Tayyebi, A.H. Analyzing long-term spatio-temporal patterns of land surface temperature in response to rapid urbanization in the mega-city of Tehran. *Land Use Policy* **2018**, *71*, 459–469. [CrossRef]
27. Peng, W.; Zhou, J.; Wen, L.; Xue, S.; Dong, L. Land surface temperature and its impact factors in Western Sichuan Plateau, China. *Geocarto Int.* **2017**, *32*, 919–934. [CrossRef]
28. Heinl, M.; Hammerle, A.; Tappeiner, U.; Leitinger, G. Determinants of urban–rural land surface temperature differences–A landscape scale perspective. *Landsc. Urban Plan.* **2015**, *134*, 33–42. [CrossRef]
29. Kiavarz, M.; Hosseinbeigi, S.B.; Mijani, N.; Shahsavary, M.S.; Firozjaei, M.K. Predicting spatial and temporal changes in surface urban heat islands using multi-temporal satellite imagery: A case study of Tehran metropolis. *Urban Clim.* **2022**, *45*, 101258. [CrossRef]
30. Nadizadeh Shorabeh, S.; Hamzeh, S.; Zanganeh Shahraki, S.; Firozjaei, M.K.; Jokar Arsanjani, J. Modelling the intensity of surface urban heat island and predicting the emerging patterns: Landsat multi-temporal images and Tehran as case study. *Int. J. Remote Sens.* **2020**, *41*, 7400–7426. [CrossRef]
31. Firozjaei, M.K.; Kiavarz, M.; Alavipanah, S.K.; Lakes, T.; Qureshi, S. Monitoring and forecasting heat island intensity through multi-temporal image analysis and cellular automata-Markov chain modelling: A case of Babol city, Iran. *Ecol. Indic.* **2018**, *91*, 155–170. [CrossRef]
32. Tian, P.; Li, J.; Cao, L.; Pu, R.; Wang, Z.; Zhang, H.; Chen, H.; Gong, H. Assessing spatiotemporal characteristics of urban heat islands from the perspective of an urban expansion and green infrastructure. *Sustain. Cities Soc.* **2021**, *74*, 103208. [CrossRef]
33. Li, K.; Chen, Y.; Wang, M.; Gong, A. Spatial-temporal variations of surface urban heat island intensity induced by different definitions of rural extents in China. *Sci. Total Environ.* **2019**, *669*, 229–247. [CrossRef] [PubMed]
34. Fu, P.; Weng, Q. Responses of urban heat island in Atlanta to different land-use scenarios. *Theor. Appl. Climatol.* **2018**, *133*, 123–135. [CrossRef]
35. Mathew, A.; Khandelwal, S.; Kaul, N. Spatial and temporal variations of urban heat island effect and the effect of percentage impervious surface area and elevation on land surface temperature: Study of Chandigarh city, India. *Sustain. Cities Soc.* **2016**, *26*, 264–277. [CrossRef]
36. Haashemi, S.; Weng, Q.; Darvishi, A.; Alavipanah, S.K. Seasonal variations of the surface urban heat island in a semi-arid city. *Remote Sens.* **2016**, *8*, 352. [CrossRef]
37. Firozjaei, M.K.; Fathololoumi, S.; Kiavarz, M.; Arsanjani, J.J.; Alavipanah, S.K. Modelling surface heat island intensity according to differences of biophysical characteristics: A case study of Amol city, Iran. *Ecol. Indic.* **2020**, *109*, 105816. [CrossRef]
38. Firozjaei, M.K.; Fathololoumi, S.; Mijani, N.; Kiavarz, M.; Qureshi, S.; Homaee, M.; Alavipanah, S.K. Evaluating the spectral indices efficiency to quantify daytime surface anthropogenic heat island intensity: An intercontinental methodology. *Remote Sens.* **2020**, *12*, 2854. [CrossRef]
39. Gaur, A.; Eichenbaum, M.K.; Simonovic, S.P. Analysis and modelling of surface Urban Heat Island in 20 Canadian cities under climate and land-cover change. *J. Environ. Manag.* **2018**, *206*, 145–157. [CrossRef]
40. Zhou, D.; Zhang, L.; Li, D.; Huang, D.; Zhu, C. Climate–vegetation control on the diurnal and seasonal variations of surface urban heat islands in China. *Environ. Res. Lett.* **2016**, *11*, 074009. [CrossRef]

41. Weng, Q.; Firozjaei, M.K.; Sedighi, A.; Kiavarz, M.; Alavipanah, S.K. Statistical analysis of surface urban heat island intensity variations: A case study of Babol city, Iran. *GIScience Remote Sens.* **2019**, *56*, 576–604. [CrossRef]
42. Oke, T.R. The energetic basis of the urban heat island. *Q. J. R. Meteorol. Soc.* **1982**, *108*, 1–24. [CrossRef]
43. Oke, T.R. The distinction between canopy and boundary-layer urban heat islands. *Atmosphere* **1976**, *14*, 268–277. [CrossRef]
44. Zhou, D.; Zhao, S.; Liu, S.; Zhang, L.; Zhu, C. Surface urban heat island in China's 32 major cities: Spatial patterns and drivers. *Remote Sens. Environ.* **2014**, *152*, 51–61. [CrossRef]
45. Jamei, Y.; Rajagopalan, P.; Sun, Q.C. Spatial structure of surface urban heat island and its relationship with vegetation and built-up areas in Melbourne, Australia. *Sci. Total Environ.* **2019**, *659*, 1335–1351. [CrossRef] [PubMed]
46. Wheeler, S.M.; Abunnasr, Y.; Dialesandro, J.; Assaf, E.; Agopian, S.; Gamberini, V.C. Mitigating urban heating in dryland cities: A literature review. *J. Plan. Lit.* **2019**, *34*, 434–446. [CrossRef]
47. Alahmad, B.; Tomasso, L.P.; Al-Hemoud, A.; James, P.; Koutrakis, P. Spatial distribution of land surface temperatures in Kuwait: Urban heat and cool islands. *Int. J. Environ. Res. Public Health* **2020**, *17*, 2993. [CrossRef]
48. Moffett, K.B.; Makido, Y.; Shandas, V. Urban-rural surface temperature deviation and intra-urban variations contained by an urban growth boundary. *Remote Sens.* **2019**, *11*, 2683. [CrossRef]
49. Dialesandro, J.M.; Wheeler, S.M.; Abunnasr, Y. Urban heat island behaviors in dryland regions. *Environ. Res. Commun.* **2019**, *1*, 081005. [CrossRef]
50. Rasul, A.; Balzter, H.; Smith, C. Spatial variation of the daytime Surface Urban Cool Island during the dry season in Erbil, Iraqi Kurdistan, from Landsat 8. *Urban Clim.* **2015**, *14*, 176–186. [CrossRef]
51. Masoodian, S.A.; Montazeri, M. Quantifying of surface urban cool island in arid environments case study: Isfahan metropolis. *Landsc. Ecol. Eng.* **2021**, *17*, 147–156. [CrossRef]
52. Govind, N.R.; Ramesh, H. The impact of spatiotemporal patterns of land use land cover and land surface temperature on an urban cool island: A case study of Bengaluru. *Environ. Monit. Assess.* **2019**, *191*, 283. [CrossRef] [PubMed]
53. Akinyemi, F.O.; Ikanyeng, M.; Muro, J. Land cover change effects on land surface temperature trends in an African urbanizing dryland region. *City Environ. Interact.* **2019**, *4*, 100029. [CrossRef]
54. Li, X.; Zhou, Y.; Zhu, Z.; Liang, L.; Yu, B.; Cao, W. Mapping annual urban dynamics (1985–2015) using time series of Landsat data. *Remote Sens. Environ.* **2018**, *216*, 674–683. [CrossRef]
55. Sun, Y.; Gao, C.; Li, J.; Wang, R.; Liu, J. Quantifying the effects of urban form on land surface temperature in subtropical high-density urban areas using machine learning. *Remote Sens.* **2019**, *11*, 959. [CrossRef]
56. Jiménez-Muñoz, J.C.; Cristóbal, J.; Sobrino, J.A.; Sòria, G.; Ninyerola, M.; Pons, X. Revision of the single-channel algorithm for land surface temperature retrieval from Landsat thermal-infrared data. *IEEE Trans. Geosci. Remote Sens.* **2009**, *47*, 339–349. [CrossRef]
57. Jiménez-Muñoz, J.C.; Sobrino, J.A. A generalized single-channel method for retrieving land surface temperature from remote sensing data. *J. Geophys. Res. Atmos.* **2003**, *108*, 4688. [CrossRef]
58. Li, Z.-L.; Tang, B.-H.; Wu, H.; Ren, H.; Yan, G.; Wan, Z.; Trigo, I.F.; Sobrino, J.A. Satellite-derived land surface temperature: Current status and perspectives. *Remote Sens. Environ.* **2013**, *131*, 14–37. [CrossRef]
59. Bian, Z.; Fan, T.; Roujean, J.-L.; Wang, D.; Irvine, M.; Wu, S.; Cao, B.; Li, H.; Du, Y.; Xiao, Q. An analytical urban temperature model with building heterogeneity using geometric optical theory. *Remote Sens. Environ.* **2024**, *301*, 113948. [CrossRef]
60. Firozjaei, M.K.; Weng, Q.; Zhao, C.; Kiavarz, M.; Lu, L.; Alavipanah, S.K. Surface anthropogenic heat islands in six megacities: An assessment based on a triple-source surface energy balance model. *Remote Sens. Environ.* **2020**, *242*, 111751. [CrossRef]
61. Coutts, A.M.; Harris, R.J.; Phan, T.; Livesley, S.J.; Williams, N.S.; Tapper, N.J. Thermal infrared remote sensing of urban heat: Hotspots, vegetation, and an assessment of techniques for use in urban planning. *Remote Sens. Environ.* **2016**, *186*, 637–651. [CrossRef]
62. Dar, I.; Qadir, J.; Shukla, A. Estimation of LST from multi-sensor thermal remote sensing data and evaluating the influence of sensor characteristics. *Ann. GIS* **2019**, *25*, 263–281. [CrossRef]
63. Chrysoulakis, N. Estimation of the all-wave urban surface radiation balance by use of ASTER multispectral imagery and in situ spatial data. *J. Geophys. Res. Atmos.* **2003**, *108*, 4582. [CrossRef]
64. Liu, L.; Zhang, Y. Urban heat island analysis using the Landsat TM data and ASTER data: A case study in Hong Kong. *Remote Sens.* **2011**, *3*, 1535–1552. [CrossRef]
65. Kato, S.; Yamaguchi, Y. Estimation of storage heat flux in an urban area using ASTER data. *Remote Sens. Environ.* **2007**, *110*, 1–17. [CrossRef]
66. Liu, H.; Weng, Q. Scaling effect of fused ASTER-MODIS land surface temperature in an urban environment. *Sensors* **2018**, *18*, 4058. [CrossRef] [PubMed]
67. Wang, D.; Chen, Y.; Hu, L.; Voogt, J.A.; Gastellu-Etchegorry, J.-P.; Krayenhoff, E.S. Modeling the angular effect of MODIS LST in urban areas: A case study of Toulouse, France. *Remote Sens. Environ.* **2021**, *257*, 112361. [CrossRef]
68. Weng, Q.; Firozjaei, M.K.; Kiavarz, M.; Alavipanah, S.K.; Hamzeh, S. Normalizing land surface temperature for environmental parameters in mountainous and urban areas of a cold semi-arid climate. *Sci. Total Environ.* **2019**, *650*, 515–529. [CrossRef]
69. Chang, Y.; Xiao, J.; Li, X.; Middel, A.; Zhang, Y.; Gu, Z.; Wu, Y.; He, S. Exploring diurnal thermal variations in urban local climate zones with ECOSTRESS land surface temperature data. *Remote Sens. Environ.* **2021**, *263*, 112544. [CrossRef]

70. Rajasekar, U.; Weng, Q. Urban heat island monitoring and analysis using a non-parametric model: A case study of Indianapolis. *Isprs J. Photogramm.* **2009**, *64*, 86–96. [CrossRef]
71. Nichol, J. An emissivity modulation method for spatial enhancement of thermal satellite images in urban heat island analysis. *Photogramm. Eng. Remote Sens.* **2009**, *75*, 547–556. [CrossRef]
72. Gallo, K.P.; Owen, T.W. Satellite-based adjustments for the urban heat island temperature bias. *J. Appl. Meteorol.* **1999**, *38*, 806–813. [CrossRef]
73. Liu, X.; Zhou, Y.; Yue, W.; Li, X.; Liu, Y.; Lu, D. Spatiotemporal patterns of summer urban heat island in Beijing, China using an improved land surface temperature. *J. Clean. Prod.* **2020**, *257*, 120529. [CrossRef]
74. Chen, S.; Hu, D.; Wong, M.S.; Ren, H.; Cao, S.; Yu, C.; Ho, H.C. Characterizing spatiotemporal dynamics of anthropogenic heat fluxes: A 20-year case study in Beijing–Tianjin–Hebei region in China. *Environ. Pollut.* **2019**, *249*, 923–931. [CrossRef] [PubMed]
75. Meng, Q.; Zhang, L.; Sun, Z.; Meng, F.; Wang, L.; Sun, Y. Characterizing spatial and temporal trends of surface urban heat island effect in an urban main built-up area: A 12-year case study in Beijing, China. *Remote Sens. Environ.* **2018**, *204*, 826–837. [CrossRef]
76. Firozjaei, M.K.; Kiavarz, M.; Alavipanah, S.K. Monitoring and predicting spatial-temporal changes heat island in Babol city due to urban sprawl and land use changes. *J. Geospat. Inf. Technol.* **2017**, *5*, 123–151. [CrossRef]
77. Alavipanah, S.K.; Kiavarz, M.; Firozjaei, M.K. Monitoring spatiotemporal changes of heat island in babol city due to land use changes. *Int. Arch. Photogramm. Remote Sens. Spat. Inf. Sci.* **2017**, *42*, 17–22. [CrossRef]
78. Van Hove, L.; Jacobs, C.; Heusinkveld, B.; Elbers, J.; Van Driel, B.; Holtslag, A. Temporal and spatial variability of urban heat island and thermal comfort within the Rotterdam agglomeration. *Build. Environ.* **2015**, *83*, 91–103. [CrossRef]
79. Ramírez-Aguilar, E.A.; Souza, L.C.L. Urban form and population density: Influences on Urban Heat Island intensities in Bogotá, Colombia. *Urban Clim.* **2019**, *29*, 100497. [CrossRef]
80. Huang, X.; Wang, Y. Investigating the effects of 3D urban morphology on the surface urban heat island effect in urban functional zones by using high-resolution remote sensing data: A case study of Wuhan, Central China. *ISPRS J. Photogramm. Remote Sens.* **2019**, *152*, 119–131. [CrossRef]
81. Zhou, B.; Rybski, D.; Kropp, J.P. The role of city size and urban form in the surface urban heat island. *Sci. Rep.* **2017**, *7*, 4791. [CrossRef]
82. Singh, P.; Kikon, N.; Verma, P. Impact of land use change and urbanization on urban heat island in Lucknow city, Central India. A remote sensing based estimate. *Sustain. Cities Soc.* **2017**, *32*, 100–114. [CrossRef]
83. Bahi, H.; Rhinane, H.; Bensalmia, A.; Fehrenbach, U.; Scherer, D. Effects of urbanization and seasonal cycle on the surface urban heat island patterns in the coastal growing cities: A case study of Casablanca, Morocco. *Remote Sens.* **2016**, *8*, 829. [CrossRef]
84. Rotem-Mindali, O.; Michael, Y.; Helman, D.; Lensky, I.M. The role of local land-use on the urban heat island effect of Tel Aviv as assessed from satellite remote sensing. *Appl. Geogr.* **2015**, *56*, 145–153. [CrossRef]
85. Wu, Z.; Zhang, Y. Water Bodies' Cooling Effects on Urban Land Daytime Surface Temperature: Ecosystem Service Reducing Heat Island Effect. *Sustainability* **2019**, *11*, 787. [CrossRef]
86. Li, X.; Zhou, W. Optimizing urban greenspace spatial pattern to mitigate urban heat island effects: Extending understanding from local to the city scale. *Urban For. Urban Green.* **2019**, *41*, 255–263. [CrossRef]
87. Mackey, C.W.; Lee, X.; Smith, R.B. Remotely sensing the cooling effects of city scale efforts to reduce urban heat island. *Build. Environ.* **2012**, *49*, 348–358. [CrossRef]
88. Rahman, M.T.; Aldosary, A.S.; Mortoja, M. Modeling future land cover changes and their effects on the land surface temperatures in the Saudi Arabian eastern coastal city of Dammam. *Land* **2017**, *6*, 36. [CrossRef]
89. Mushore, T.D.; Odindi, J.; Dube, T.; Mutanga, O. Prediction of future urban surface temperatures using medium resolution satellite data in Harare metropolitan city, Zimbabwe. *Build. Environ.* **2017**, *122*, 397–410. [CrossRef]
90. Ahmed, B.; Kamruzzaman, M.; Zhu, X.; Rahman, M.; Choi, K. Simulating land cover changes and their impacts on land surface temperature in Dhaka, Bangladesh. *Remote Sens.* **2013**, *5*, 5969–5998. [CrossRef]
91. Liu, J.; Zhang, L.; Zhang, Q.; Zhang, G.; Teng, J. Predicting the surface urban heat island intensity of future urban green space development using a multi-scenario simulation. *Sustain. Cities Soc.* **2021**, *66*, 102698. [CrossRef]
92. Singla, S.K.; Garg, R.D.; Dubey, O.P. Sugarcane ratoon discrimination using LANDSAT NDVI temporal data. *Spat. Inf. Res.* **2018**, *26*, 415–425. [CrossRef]
93. Myroniuk, V. Forest cover mapping using Landsat-based seasonal composited mosaics. *Sci. Bull. UNFU* **2018**, *28*, 28–33. [CrossRef]
94. Son, N.-T.; Chen, C.-F.; Chen, C.-R.; Thanh, B.-X.; Vuong, T.-H. Assessment of urbanization and urban heat islands in Ho Chi Minh City, Vietnam using Landsat data. *Sustain. Cities Soc.* **2017**, *30*, 150–161. [CrossRef]
95. Peña, M.; Brenning, A. Assessing fruit-tree crop classification from Landsat-8 time series for the Maipo Valley, Chile. *Remote Sens. Environ.* **2015**, *171*, 234–244. [CrossRef]
96. Jin, X.; Ma, J.; Wen, Z.; Song, K. Estimation of maize residue cover using Landsat-8 OLI image spectral information and textural features. *Remote Sens.* **2015**, *7*, 14559–14575. [CrossRef]
97. Qin, Q.; Zhang, N.; Nan, P.; Chai, L. Geothermal area detection using Landsat ETM+ thermal infrared data and its mechanistic analysis—A case study in Tengchong, China. *Int. J. Appl. Earth Obs. Geoinf.* **2011**, *13*, 552–559. [CrossRef]
98. Belgiu, M.; Drăguţ, L. Random forest in remote sensing: A review of applications and future directions. *ISPRS J. Photogramm. Remote Sens.* **2016**, *114*, 24–31. [CrossRef]

99. Gislason, P.O.; Benediktsson, J.A.; Sveinsson, J.R. Random forests for land cover classification. *Pattern Recognit. Lett.* **2006**, *27*, 294–300. [CrossRef]
100. Pal, M. Random forest classifier for remote sensing classification. *Int. J. Remote Sens.* **2005**, *26*, 217–222. [CrossRef]
101. Fu, X.; Wang, X.; Yang, Y.J. Deriving suitability factors for CA-Markov land use simulation model based on local historical data. *J. Environ. Manag.* **2018**, *206*, 10–19. [CrossRef]
102. Liu, Y.; Dai, L.; Xiong, H. Simulation of urban expansion patterns by integrating auto-logistic regression, Markov chain and cellular automata models. *J. Environ. Plan. Manag.* **2015**, *58*, 1113–1136. [CrossRef]
103. Guan, D.; Li, H.; Inohae, T.; Su, W.; Nagaie, T.; Hokao, K. Modeling urban land use change by the integration of cellular automaton and Markov model. *Ecol. Model.* **2011**, *222*, 3761–3772. [CrossRef]
104. Arsanjani, J.J.; Helbich, M.; Kainz, W.; Boloorani, A.D. Integration of logistic regression, Markov chain and cellular automata models to simulate urban expansion. *Int. J. Appl. Earth Obs.* **2013**, *21*, 265–275. [CrossRef]
105. Firozjaei, M.K.; Sedighi, A.; Argany, M.; Jelokhani-Niaraki, M.; Arsanjani, J.J. A geographical direction-based approach for capturing the local variation of urban expansion in the application of CA-Markov model. *Cities* **2019**, *93*, 120–135. [CrossRef]
106. Harker, P.T.; Vargas, L.G. The theory of ratio scale estimation: Saaty's analytic hierarchy process. *Manag. Sci.* **1987**, *33*, 1383–1403. [CrossRef]
107. Aragonés-Beltrán, P.; Chaparro-González, F.; Pastor-Ferrando, J.-P.; Pla-Rubio, A. An AHP (Analytic Hierarchy Process)/ANP (Analytic Network Process)-based multi-criteria decision approach for the selection of solar-thermal power plant investment projects. *Energy* **2014**, *66*, 222–238. [CrossRef]
108. Tucker, C.J. Red and photographic infrared linear combinations for monitoring vegetation. *Remote Sens. Environ.* **1979**, *8*, 127–150. [CrossRef]
109. Zha, Y.; Gao, J.; Ni, S. Use of normalized difference built-up index in automatically mapping urban areas from TM imagery. *Int. J. Remote Sens.* **2003**, *24*, 583–594. [CrossRef]
110. Gao, B.-C. NDWI—A normalized difference water index for remote sensing of vegetation liquid water from space. *Remote Sens. Environ.* **1996**, *58*, 257–266. [CrossRef]
111. Firozjaei, M.K.; Sedighi, A.; Firozjaei, H.K.; Kiavarz, M.; Homaee, M.; Arsanjani, J.J.; Makki, M.; Naimi, B.; Alavipanah, S.K. A historical and future impact assessment of mining activities on surface biophysical characteristics change: A remote sensing-based approach. *Ecol. Indic.* **2021**, *122*, 107264. [CrossRef]
112. Wang, Q.; Guan, Q.; Lin, J.; Luo, H.; Tan, Z.; Ma, Y. Simulating land use/land cover change in an arid region with the coupling models. *Ecol. Indic.* **2021**, *122*, 107231. [CrossRef]
113. Arshad, S.; Hasan Kazmi, J.; Fatima, M.; Khan, N. Change detection of land cover/land use dynamics in arid region of Bahawalpur District, Pakistan. *Appl. Geomat.* **2022**, *14*, 387–403. [CrossRef]
114. Duraisamy, V.; Bendapudi, R.; Jadhav, A. Identifying hotspots in land use land cover change and the drivers in a semi-arid region of India. *Environ. Monit. Assess.* **2018**, *190*, 535. [CrossRef] [PubMed]
115. Ren, J.; Zhou, W.; Liu, X.; Zhou, L.; Guo, J.; Wang, Y.; Guan, Y.; Mao, J.; Huang, Y.; Ma, R. Urban Expansion and growth boundaries in an Oasis City in an arid region: A case study of Jiayuguan City, China. *Sustainability* **2019**, *12*, 210. [CrossRef]
116. Pan, T.; Lu, D.; Zhang, C.; Chen, X.; Shao, H.; Kuang, W.; Chi, W.; Liu, Z.; Du, G.; Cao, L. Urban land-cover dynamics in arid China based on high-resolution urban land mapping products. *Remote Sens.* **2017**, *9*, 730. [CrossRef]
117. Mansour, S.; Alahmadi, M.; Atkinson, P.M.; Dewan, A. Forecasting of built-up land expansion in a desert urban environment. *Remote Sens.* **2022**, *14*, 2037. [CrossRef]
118. Rida, A.; KOUMETIO, C.S.T.; Diop, E.B.; Chenal, J. Exploring the relationship between urban form and land surface temperature (LST) in a semi-arid region Case study of Ben Guerir city-Morocco. *Environ. Chall.* **2021**, *5*, 100229.
119. Abulibdeh, A. Analysis of urban heat island characteristics and mitigation strategies for eight arid and semi-arid gulf region cities. *Environ. Earth Sci.* **2021**, *80*, 259. [CrossRef]
120. Parvez, I.M.; Aina, Y.A.; Balogun, A.-L. The influence of urban form on the spatiotemporal variations in land surface temperature in an arid coastal city. *Geocarto Int.* **2021**, *36*, 640–659. [CrossRef]
121. Peng, S.; Piao, S.; Ciais, P.; Friedlingstein, P.; Ottle, C.; Bréon, F.-M.; Nan, H.; Zhou, L.; Myneni, R.B. Surface urban heat island across 419 global big cities. *Environ. Sci. Technol.* **2012**, *46*, 696–703. [CrossRef]
122. Lazzarini, M.; Marpu, P.R.; Ghedira, H. Temperature-land cover interactions: The inversion of urban heat island phenomenon in desert city areas. *Remote Sens. Environ.* **2013**, *130*, 136–152. [CrossRef]
123. Saaroni, H.; Bitan, A.; Dor, E.B.; Feller, N. The mixed results concerning the 'oasis effect' in a rural settlement in the Negev Desert, Israel. *J. Arid Environ.* **2004**, *58*, 235–248. [CrossRef]
124. Ganbat, G.; Han, J.-Y.; Ryu, Y.-H.; Baik, J.-J. Characteristics of the urban heat island in a high-altitude metropolitan city, Ulaanbaatar, Mongolia. *Asia-Pac. J. Atmos. Sci.* **2013**, *49*, 535–541. [CrossRef]
125. Imhoff, M.L.; Zhang, P.; Wolfe, R.E.; Bounoua, L. Remote sensing of the urban heat island effect across biomes in the continental USA. *Remote Sens. Environ.* **2010**, *114*, 504–513. [CrossRef]

Disclaimer/Publisher's Note: The statements, opinions and data contained in all publications are solely those of the individual author(s) and contributor(s) and not of MDPI and/or the editor(s). MDPI and/or the editor(s) disclaim responsibility for any injury to people or property resulting from any ideas, methods, instructions or products referred to in the content.